UNIVERSITY OF OKLAHOMA

GRADUATE COLLEGE

Feedback Models and Bursty Star Formation Histories in Dwarf Galaxies

A THESIS

SUBMITTED TO THE GRADUATE FACULTY

in partial fulfillment of the requirements for the

Degree of

MASTER OF SCIENCE

By

BIANCA C AZARTASH-NAMIN
Norman, Oklahoma
2024

FEEDBACK MODELS AND BURSTY STAR FORMATION HISTORIES IN DWARF GALAXIES

A THESIS APPROVED FOR THE
HOMER L. DODGE DEPARTMENT OF PHYSICS AND ASTRONOMY

BY THE COMMITTEE CONSISTING OF

Dr. Mukremin Kilic, Chair

Dr. Ferah Munshi

Dr. Sean Matt

Dedication

For my Son;

Per Aspera Ad Astra

Acknowledgements

I am thankful for the endless love and support from my family, which has allowed me to pursue my education and persevere in achieving my professional goals. Without their sacrifices and encouragement, my academic career and the culmination of this work would not have been possible.

To my partner, Anthony, thank you for being my guiding light. Your companionship, advice, and unconditional support were the reminders I needed to keep going, even when I doubted myself and the journey felt impossible. Your presence in my life gives me the strength and motivation to move forward, and I will carry your love and support into the next chapter of my life.

To my advisor, Mukremin Kilic, thank you for your endless support and kindness. I could not have succeeded as a graduate student without your guidance and encouragement. I also extend my gratitude to the other members of my committee, Ferah Munshi and Sean Matt, for their invaluable expertise throughout my graduate career. Their insights and feedback greatly shaped the direction of my research, and I deeply appreciate the time they dedicated to reviewing my work. Additionally, I would like to thank Nate Kaib and John Stupak for their mentorship during my years at OU. I am sincerely grateful for their professional guidance and personal support.

I would also like to thank my colleagues and friends from my time at OU, including Amber, Jon Dale, Alexi, Stephanie, Chanun, and many others. Your love and support have been an endless source of inspiration. I am especially grateful to members of my research group, Anna and Jordan, for their unwavering support and exceptional teamwork. I wish them the utmost success in all their personal and professional endeavors.

Finally, I would like to extend my heartfelt thanks to my collaborators, whose support and expertise were invaluable to the completion of this work. I would especially like to thank Ferah Munshi, Ben Keller, Charlotte Christensen, and Alyson Brooks for sharing their expertise and resources that were instrumental in both this work and my professional career as a whole. I am also grateful to the N-Body Shop collaboration for allowing me to work alongside such talented and dedicated individuals, which has been an inspiring and rewarding experience.

Contents

Abstract

To address tensions between DM-only simulations and observations on smaller scales, simulations implementing baryonic feedback have successfully produced galaxies with "cored" DM density profiles that are observed in nature and in conflict with the "cuspy" profiles predicted by Λ for low-mass galaxies. The goal of this thesis is to address this cusp-core problem for ΛCDM simulations by introducing a robust comparison of the relationship between bursty star formation, or burstiness, and DM cores using two distinct SN feedback models with different sub-grid physics. This work analyzes two runs of the Storm simulation from the MARVEL suite of dwarf galaxies (one with blastwave feedback and one with superbubble feedback) by calculating various forms of burstiness for the Storm dwarf galaxies and comparing them to the DM density profile of the corresponding DM halo. This is achieved by comparing burstiness and DM core slopes, or the variation of the density profile for a chosen radial distance from the center of the galaxy, over the entire cosmic timescale and the time period of active star formation for each halo to determine that DM core formation and sustainment is correlated to higher values of burstiness.

This work finds that there is a general trend between burstiness and the DM density profile, and that DM cores are efficiently sustained in the higher dwarf galaxy mass regime where star formation is burstier while the majority of ultra-faint and classical dwarf galaxies retain cuspy central DM density profiles regardless of feedback model. In addition, this work quantifies how strongly burstiness and DM core slopes depend on the stellar mass fraction, M_*/M_{halo}, and finds that core formation may be better predicted by M_*/M_{halo} than burstiness as peak core formation occurs at different values of the stellar mass fraction for a given feedback model. Testing the robustness of the burstiness and core slope relation in this work improves our understanding of the cusp-core problem under the ΛCDM paradigm by constraining cored DM profiles to the higher dwarf galaxy mass regime and provides observational predictions on the SFHs and density profiles of classical dwarfs and UFDs that are expected to increase in discovery with upcoming surveys from the James Webb Space Telescope (JWST), Vera Rubin Observatory (VRO), and the Nancy Grace Roman Space Telescope (Roman).

CHAPTER 1

Introduction

The Universe is vast and complex with a diverse assortment of structures that form and evolve differently. These structures, ranging from smaller stars and planets to massive galaxies and galaxy clusters, are all interconnected by a cosmic web of DM that drives their large-scale formation. As the Universe is approximately 13.8 billion years old (Bennett et al., 2013) and expanding, it is impossible to understand the origin and evolution of structures over time without theoretical frameworks and models. The ΛCDM paradigm is the standard framework to describe the nature of the Universe, explain fundamental physical processes, and support astronomical observations across the entire cosmic timescale.

Under this paradigm, the ΛCDM model unifies ordinary (baryonic) matter, DM, and dark energy. These components interact and evolve over time to produce what is observed today across different scales and epochs of the Universe. This model accurately describes how large-scale structures form, the hierarchy of structure formation, and the evolution of the Universe from the Big Bang using the effects of these components (Eisenstein & Hu, 1998; Guth, 1981; Hu & White, 2004; Baumann, 2009). However, it also raises profound questions about the nature of DM and dark energy and introduces challenges on smaller scales. DM-only simulations face several tensions with observation, including the cusp-core problem (Flores & Primack, 1994; Moore, 1994; Governato et al., 2010a), the missing satellites problem (Klypin et al., 1999; Moore et al., 1999), and the too-big-to-fail problem (Boylan-Kolchin et al., 2011, 2012). These issues necessitate modifications or new physics to the ΛCDM model to be successful across all scales.

1.1. Cosmological Paradigms

To better understand why small-scale structures need to be treated differently under modern cosmology, it is important to consider how the Universe is modeled and compares to observational data. Cosmological modeling involves various paradigms with key differences in physical principles and assumptions to describe the large-scale structure and evolution of the universe.

The Universe is described as dominated by dark energy (Λ) and made up of cold dark matter (CDM), baryons, and contributions from radiation (Peebles & Ratra, 1988). Observational data supports a Universe comprised of $\sim 70\%$ dark energy, $\sim 25\%$ CDM, and only $\sim 5\%$ of the total energy distribution from baryonic matter that forms all visible structures. The ΛCDM model is the current standard paradigm in cosmology for incorporating these features under the Cosmological

Principle, in which the Universe is assumed homogeneous and isotropic on large scales. Additionally, this model obeys the Friedmann equations from General Relativity (GR) to describe the expansion of the Universe and incorporates inflation, Big Bang nucleosynthesis, large-scale structure formation, and the Cosmic Microwave Background (CMB) (Lemaitre, 1934; Penzias & Wilson, 1965; Alpher et al., 1948; Guth, 1981).

Einstein (1917) introduced the cosmological constant Λ as an additional term in GR to represent a constant energy density that fills space homogeneously. In modern cosmology, this constant is interpreted as dark energy that acts as a driving force for the accelerated expansion of the Universe and contributes approximately 70% of the total energy density of the Universe according to observed data from Type Ia supernovae (SNe) and the CMB (Riess et al., 1998; Perlmutter et al., 1999; Planck Collaboration et al., 2020). Observationally, this acceleration measures 10^{-122} in natural (Planck) units, which corresponds to an extremely small energy density of the vacuum of space (Schmidt, 2012). However, theoretical predictions in quantum field theory (QFT) expect this value to be 10^{120} times larger than the observed value (Schmidt, 2012), leading to a discrepancy between observation and the calculation of energy density based on quantum mechanics and special relativity (Weinberg, 1989). As a result, alternative models have been pursued to explain dark energy without invoking the cosmological constant despite the success of the ΛCDM model to address a wide range of cosmological observations.

Modified gravity theories attempt to extend GR to explain cosmic acceleration and dark energy with generalized functions or predict higher-dimensional space that alters gravity at cosmological scales. However, this framework faces challenges in reaching a consensus on an emergent modified gravity model that is applicable to all relevant scales. In addition, modified gravity theories lack an ability to reproduce cosmological observations at the same scales achieved by ΛCDM. This model fails to fit both large-scale structures and crucial properties of the CMB that require a precise temperature, uniformity, and polarization anisotropies (Linder, 2017; Planck Collaboration et al., 2020; Shankaranarayanan & Johnson, 2022).

Inhomogeneous cosmologies attribute cosmic acceleration and dark energy to the effects of large-scale structures and propose that cosmic inhomogeneities such as voids and clusters contribute to the dynamics and expansion of the Universe (Buchert, 2000). Although this model provides explanations for conditions of the early Universe, it also introduces significant mathematical and computational complexities and complicates the distribution of DM at various scales. This not only limits the predictive power and usability of this model, but it also fails to address well-supported evidence of homogeneity and isotropy of cosmological observations. Galaxy surveys and the CMB show evidence that the Universe behaves similarly between small and large scales (Tegmark et al., 2004; Efstathiou et al., 2002), further negating the relevance of inhomogeneous modeling of local and global effects on cosmological measurements.

1.1.1. Λ Cold Dark Matter

As introduced in Section 1.1, ΛCDM is a framework that includes two key components — dark energy Λ that dominates the Universe and drives cosmic expansion, and cold dark matter (CDM). CDM is described by DM particles that are collisionless and propagate slowly relative to the speed of light, making them "cold." CDM particles are non-baryonic and only interact with other particles through gravity. As a result, CDM particles interact weakly and do not exhibit the same scatter and collision behavior of baryonic particle interactions such as protons, neutrons, or electrons that interact with contributions from electromagnetic or nuclear forces. In addition, CDM particles are expected to be stable and long-lived on cosmological timescales, as they do not decay into other particles.

CDM plays a crucial role in the hierarchical growth of cosmological structures (Peebles, 1980a). As discussed in Chapter 1.1, the ΛCDM model of cosmology operates within the framework of general relativity to describe the physics of structure formation and additionally relies on particle physics and astrophysics to understand the particle nature of DM. After the Big Bang, the hot and uniformly dense Universe entered a period of rapid expansion, known as cosmic inflation, in which small density perturbations occurred. Throughout the age of the Universe, these perturbations became more prominent under the influence of the gravitational potential from DM, allowing ordinary matter particles to form stars, galaxies, and other luminous structures observed today. To understand the evolution of density perturbations that began during cosmic inflation, Mo et al. (2010) define a power spectrum

$$P(k) \propto k^n, \tag{1.1}$$

where k is a wave number given by $k = 2\pi/\lambda$ and therefore inversely proportional to the wavelength of the perturbation, λ. The value of k then corresponds to different physical scales, where small k deals with perturbations over larger scales and large k represent small-scale structures. However, as the Universe evolves, the power spectrum is modified to include the growth of these density perturbations which can be expressed as

$$P(k) \propto T^2(k) \tag{1.2}$$

where $T^2(k)$ is the transfer function that accounts for changes to the density perturbations throughout the age of the Universe and is proportional to the initial power spectrum (Mo et al., 2010). As the transfer function is also a function of k, this adaptation of the power spectrum still applies to different physical scales, where small k applies to perturbations on larger scales, and larger values of k encompass perturbations on smaller scales. The importance of this is illustrated in Figure 1.1, where the power spectrum is plotted as a function of wave number on the bottom axis. At

$\Delta = 1$, the power spectrum representing the evolution of density perturbations is no longer growing linearly, and as result, large perturbations form dense regions that ultimately become DM halos where galaxies begin to form. DM halos will be discussed in detail in the following section.

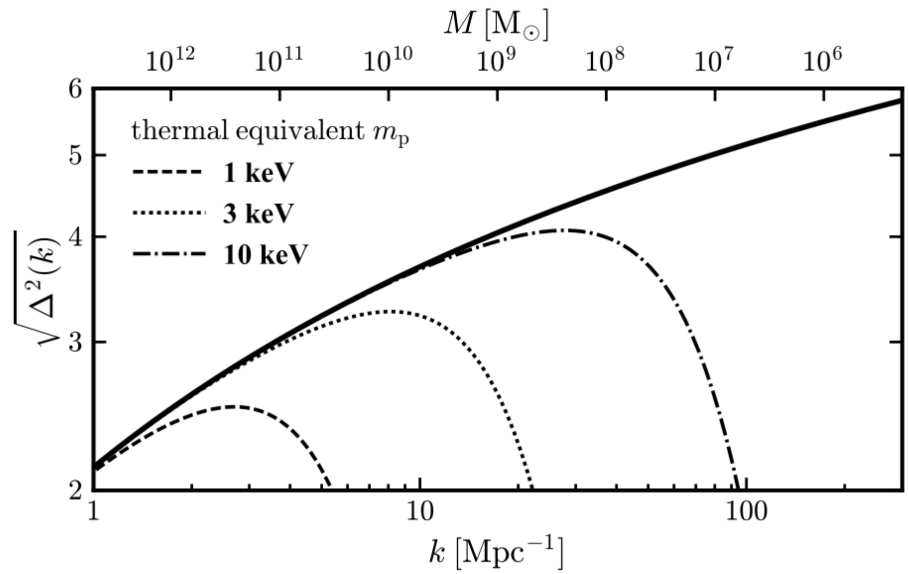

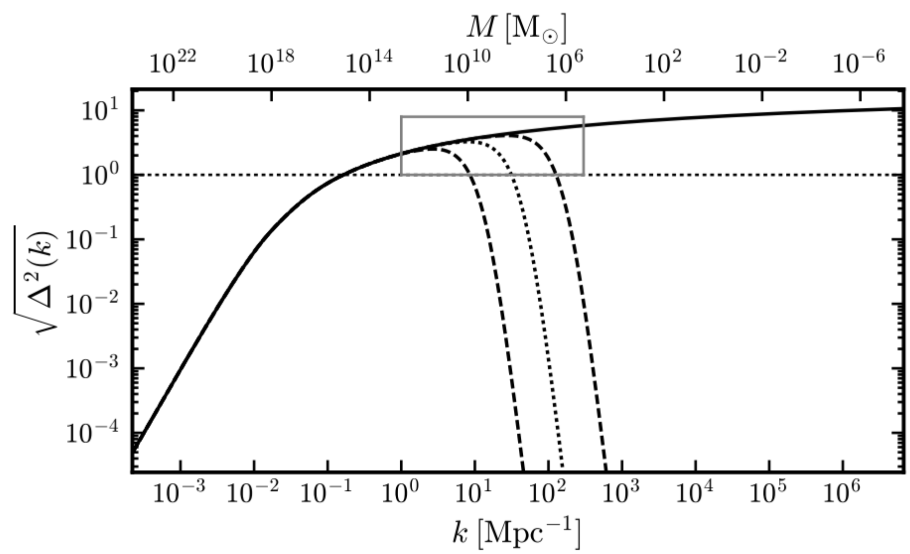

Figure 1.1: The ΛCDM power spectrum (solid lines; Equation 1.2) plot from Bullock & Boylan-Kolchin (2017) as a function of k (bottom axis). At $\Delta = 1$, the power spectrum representing the evolution of density perturbations is no longer growing linearly, which means that dense regions begin to form DM halos and galaxies. The top panel shows a mass region corresponding to dwarf galaxies, which form after the power spectrum goes nonlinear. Bullock & Boylan-Kolchin (2017) also show alternative WDM models (see Section 2.4.1) that are represented by the dashed, dotted, and dash-dotted lines with corresponding particle masses.

The ΛCDM model currently prevails as the leading cosmological model for its ability to unify several expected parameters to describe the nature of the Universe within a simple and coherent framework, and remains unmatched in precision for successful observational predictions. Although ΛCDM is successful at predicting properties of large-scale structures, challenges to the model become prevalent on smaller scales. Bullock & Boylan-Kolchin (2017) discuss that observations on the ~ 1 Mpc scale and mass scales smaller than $\sim 10^{11}$ $M_{\odot}$ have proven difficult to reconcile with DM-only simulations of small structures such as satellite galaxies, DM subhalos, and dwarf galaxies.

The significant discrepancies between theory and observation within the ΛCDM framework will be discussed in detail in Section 2.3. To date, it is unclear whether small-scale challenges can be resolved with a better understanding of DM physics or otherwise require a fundamental revision of cosmology. These issues are addressed in various fields of active research including alternative DM models from particle physics (see Section 2.4.1) and the implementation of baryonic physics that will be discussed in Section 2.4.2. In particular, dwarf galaxy properties, DM distributions, and galaxy formation are crucial to testing CDM predictions of cosmological structure evolution and understanding the nature of DM.

1.2. Dark Matter Halos

The distribution of galaxies, clusters, and cosmic filaments that form a "cosmic web" are influenced by gravitationally bound CDM particles that drive structure formation by moving slowly and clumping together to form DM halos (White & Rees, 1978). These halos serve as the foundation for the formation of galaxies as ordinary matter particles fall into the gravitational potential wells created by CDM. These filaments of ordinary matter coalesce to form the large-scale systems observed today and are surrounded by large voids of DM.

Evidence for DM halos was fundamentally revealed by the rotation curves of galaxies, where observed rotation speeds of stars far from the galactic centers move much faster than can be explained by ordinary matter alone. Rotation curves are a visualization of the rotational velocity of stars or gas in a galaxy as a function of radial distance from the galaxy center. The velocities of stars and gas vary with distance from the center and are derived from measurements of Doppler shift in spectral lines to convey whether these objects are moving toward or away from an observer. The inner regions of galaxies have stronger gravitational forces with most of the mass concentrated at the core. As a result, rotation curves typically rise as distance increases from the center of the galaxy. Following Newtonian dynamics, velocities should decrease with distance but observations show flattened curves at large radii in spiral galaxies, indicating that mass continues to increase with radius. As the outer regions do not host the majority of a galaxy's baryonic matter, such as stars and gas, this mass must be DM extending far beyond the visible disk of the galaxy.

In 1970, Rubin & Ford (1970) measured the rotation curve of the Andromeda galaxy (M31) shown in Figure 1.2 and found that mass continues to rise beyond the last measured region at 24 kpc, indicating that DM must be present to gravitationally influence the velocities of outer stellar populations. In addition, evidence of flat rotation curves in high-luminosity spiral galaxies (Rubin et al., 1978; Peterson et al., 1978) and numerical studies of flattened galaxies (Ostriker & Peebles, 1973) collectively assert that disk galaxies must be surrounded by massive DM halos.

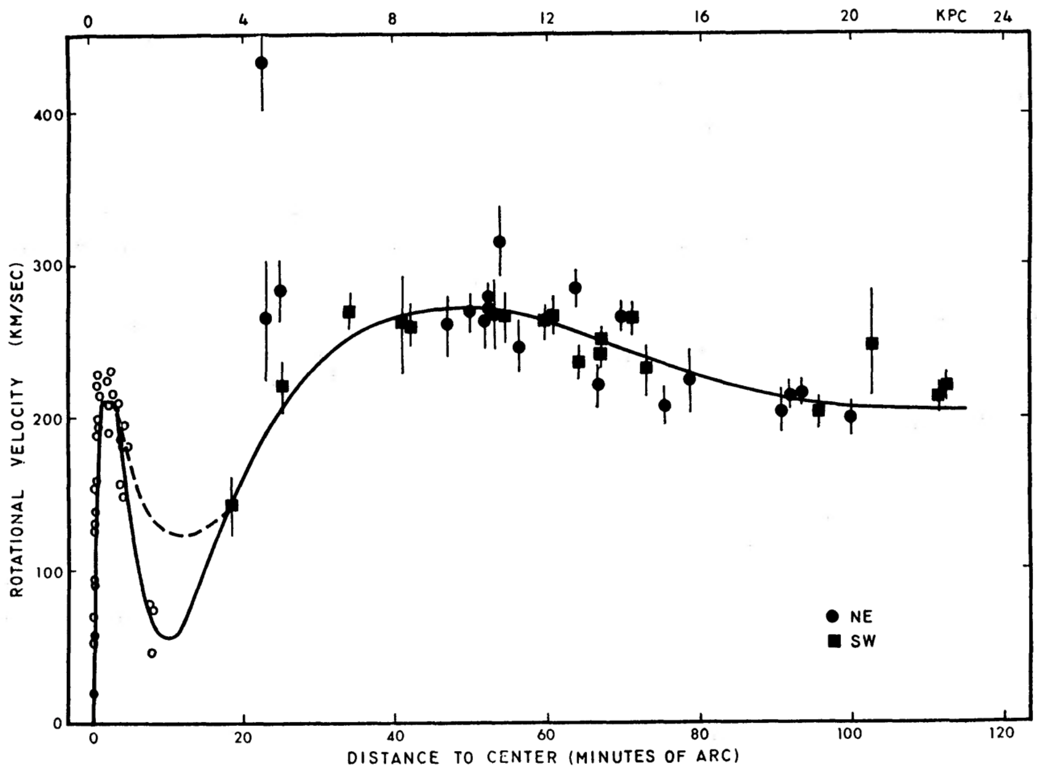

Figure 1.2: Rotational velocities of stars in M31 from the work of Rubin & Ford (1970). Stars further from the central galaxy should have slower velocities, producing a steady downward slope as the visible disk gets further away from the center. This plot instead reveals a nearly level curve beyond 24 kpc, indicating that some form of unseen mass (DM) must be present to keep the rotational velocities higher than expected.

In addition, DM dominated systems with relatively little baryonic matter, such as dwarfs, exhibit a variety of rotation curves that are shaped by the DM halo rather than stars and gas (de Blok et al., 2001). To better understand the nature of DM and how small-scale challenges are introduced in ΛCDM, it is necessary to introduce fundamental DM halo properties and address how DM is distributed within various systems. As mentioned in Section 1.1.1, over-dense regions of the Universe collapse and subsequently form "virialized" DM halos in order to reach stability. The process of virialization can be described as a system of gravitationally interacting particles that have reached a state of equilibrium and is defined by the virial theorem

$$<T>= -\frac{1}{2} <U>, \tag{1.3}$$

where $<T>$ is the averaged kinetic energy of the system and $<U>$ is the averaged gravitational potential. Hence, the virial theorem states that a system has reached dynamical equilibrium when the total kinetic energy of a system is equal to half the negative value of the total gravitational potential energy. With the assumed equations for kinetic energy and the gravitational potential for a uniform sphere of constant density,

$$T = \frac{1}{2}mv^2 \tag{1.4}$$

$$U = -\frac{3}{5}\frac{GM^2}{R} \tag{1.5}$$

the virial theorem can be arranged to generically solve for mass

$$M \approx \frac{v^2 R}{G}, \tag{1.6}$$

where M is the total mass, v is the velocity, R is the effective radius, and G is the gravitational constant. This equation is powerful in that the relation between two observable properties of galaxies (velocity dispersion and effective half-light radius) can determine a property that is unobservable — the mass of a galaxy. Consequently, the virial theorem is used for galaxy scaling relations and can be used to compare mass and luminosity estimates of galaxies to detect the presence of DM.

For spherical density perturbations that collapse into virialized DM halos, the virial mass is defined as the mass enclosed within the virial radius, or the radius at which the density is equal to the critical density (ρ_c) of the Universe for a given redshift:

$$M_{vir} = \frac{4\pi}{3} R_{vir}^3 \Delta \rho_c \tag{1.7}$$

where Δ is an over-density parameter chosen to match the predicted over-density for a DM region and defines a halo's outer edge with the virial radius, R_{vir} (Bryan & Norman, 1998). Rearranging Equation 1.8 yields the virial velocity:

$$V_{vir} = \sqrt{\frac{GM_{vir}}{R_{vir}}} \tag{1.8}$$

in which any of the individual parameters M_{vir}, R_{vir}, or V_{vir} can determine the other two. Depending on the choice of the over-density parameter, the masses of DM halos consequently vary and constrain the scale of small structures as defined by the ΛCDM power spectrum. For the purpose of this work, the over-density parameter is Δ=200, and the virial radius, $R_{riv} = 200\rho_c$, is defined as the radius at which the density is 200 times more than the critical density of the Universe. In addition, the mass scale in this work that introduces tension with the ΛCDM model is on the order of dwarf galaxies, which will be discussed in detail in Chapter 2.2.

Dubinski & Carlberg (1991) used N-body simulations (see Section 3.1.1) to reveal CDM DM halos densities do not follow a power law and scale as $\rho(r) \sim 1/r$ at small radii, indicating an inner cusp. It therefore became important to correctly model the internal structure of DM halos and how DM is distributed. DM density profiles are used to describe how the density of DM varies as a function of distance from the center of a DM halo, and are used to test cosmological models to find agreement with observational data.

1.2.1. Navarro-Frenk-White Profile

The most widely accepted profile used for simulations is the Navarro-Frenk-White (NFW) profile (Navarro et al., 1997) given by

$$\rho(r) = \frac{\rho_0}{(\frac{r}{r_s})(1+\frac{r}{r_s})^2}, \tag{1.9}$$

where ρ_0 is a characteristic density and r_s is the scale radius. In this profile, DM is predicted to be "cuspy", where the density of DM rises steeply toward the center of the halo and diverges as $\rho_r \propto r^{-1}$ near the core or center of the galaxy. At large radii, the density falls off as $\rho_r \propto r^{-3}$ which is consistent with observed DM halos on larger scales and thus successful in fitting ΛCDM predictions. As a result, the NFW profile is robust and routinely used as the standard profile used for DM-only simulations to model DM halos. However, observations of small-scale structures show deviation from the cuspy densities predicted by the NFW profile. Structures with low surface brightness indicate that the density of the central region is roughly constant or "cored."

1.2.2. Einasto Profile

Another profile applied to DM halos in simulations is the Einasto profile (Navarro et al., 2004), which is defined as

$$\rho(r) = \rho_0 \exp(-\frac{2}{\alpha}[(\frac{r}{r_s})^\alpha - 1]), \tag{1.10}$$

where α is the shape parameter that controls the steepness of the profile, and r_s is the scale radius. This profile exhibits a variable inner slope that depends on the value of α — larger values correspond to gradual density changes as a function of radius and smaller values indicate steeper changes. At the outer slope, density falls off more gradually than the NFW profile, allowing the Einasto profile to better fit the outer regions of DM halos in simulations. Additionally, the shallow inner densities are consistent with observations of systems dominated by DM in which density profiles are typically cored rather than cuspy.

1.2.3. core-Einasto Profile

A modified form of the Einasto profile, the core-Einasto profile, was introduced to better describe DM halos with flat density distributions in the central regions of certain galaxies (Lazar et al., 2020). The core-Einasto profile consists of a central core with approximately constant density and transitions to a gradual decline in density at larger radii as described by the traditional Einasto profile. As a result, the core-Einasto profile provides a better fit for dwarf and low-surface brightness galaxies. The core-Einasto profile includes a core component and the traditional Einasto function to describe the outer regions as

$$\rho(r) = \rho_0 \exp(-\frac{2}{\alpha}[(\frac{r^c + r^n}{r_s})^\alpha - 1]), \tag{1.11}$$

where α is the shape parameter, r_s is the scale radius, and the terms c and n are parameters that define the core and a transition to the outer profile. In contrast to the Einasto profile that exhibits a gradual, continuous decrease in density towards the central region, the core-Einasto profile introduces a core with an approximately constant DM density at the center. Beyond the central region, the profile transitions to the standard Einasto form with density gradually decreasing to allow for a smooth transition between the central region and outer halo where density falls off rapidly. By incorporating both a core and retaining a realistic outer halo structure, this profile has the flexibility to describe many halo types ranging from cored dwarf galaxies to massive systems that adhere to density profiles under the Einasto framework.

In summary, the core-Einasto profile is particularly useful for modeling realistic central regions of dwarf galaxies, as the observed behavior of central regions are in disagreement with the steep, cuspy profiles predicted by ΛCDM. The treatment of DM density profiles is a crucial component of simulations that addresses ΛCDM challenges and understands the DM response in small-scale structures. In this work, the core-Einasto profile is used to produce DM density cores and compared to key physical simulation processes.

1.3. Thesis Outline

This chapter has established the foundational framework of the ΛCDM model by outlining its successes in explaining the large-scale structure of the universe, as well as highlighting the small-scale challenges it faces. This background provides a basis for examining the observed DM distributions of dwarf galaxies, and how simulations are used to address the DM distribution of low-mass galaxies in the following chapters. The content of this thesis will contribute to ongoing efforts to model realistic dwarf galaxies under the ΛCDM paradigm. In particular, this work will investigate the impact of stellar feedback models in dwarf galaxy simulations by addressing the differences in subgrid physics for two distinct SN feedback methods and a novel comparison of how repeated bursts of star formation impact the formation and sustainability of DM cores within these models.

Chapter 2 discusses the classification, properties, and DM distributions of dwarfs galaxies. In addition, several key problems for the ΛCDM model will be discussed in detail and how research through dwarf galaxy simulations aims to provide solutions for these challenges by using alternative DM models or incorporating baryonic feedback.

Chapter 3 details the physics behind simulations and how baryonic feedback is incorporated to model realistic physical processes. This chapter will also introduce the simulation suite and software used in this work to model the subgrid physics of blastwave and superbubble feedback, as well as the specific star formation properties involved to model realistic dwarf galaxy evolution.

Chapter 4 describes the high resolution dwarf galaxy simulations used for the analysis of this work and expands on the implementation of baryonic feedback methodologies to highlight the physical mechanisms and sub-grid physics of the blastwave and superbubble feedback models used in separate runs of the simulations.

Chapter 5 introduces background on the concept of bursty SFHs in dwarf galaxies and describes how repeated bursts of star formation impact the formation and sustainability of DM cores within the blastwave and superbubble feedback models. This chapter will discuss how burstiness is quantified and compare the relation of burstiness and DM core formation relative to the halo masses of the dwarfs in a particular simulation suite. The implications of these results and further discussion will conclude this chapter.

Chapter 6 provides a summary of the results of this work, emphasizing the crucial role of baryonic feedback in cosmological simulations to resolve tensions between observation and the ΛCDM framework. These results will motivate the future of feedback in simulations to improve modeling realistic galaxies and better understand the interplay between feedback and the DM response.

CHAPTER 2

Dwarf Galaxies

2.1. Dwarf Galaxies and the DM Response

Dwarf galaxies are small, dark matter-dominated systems that can reveal much about the nature of DM, galaxy formation processes, and hierarchical structure formation. These galaxies are much smaller and less massive than the Milky Way galaxy (MW), typically having diameters that range from a few hundred to several thousand light-years and a diverse range of stellar masses. Dwarf galaxies are also faint, with luminosities that can be up to a thousand times fainter than the MW and can be particularly difficult to detect as they are dominated by DM. Due to the low gravitational potential of dwarfs, feedback processes such as SNe driven winds strip the gas within the galaxy and quench star formation.

As the majority of their total mass is DM, dwarf galaxies serve as excellent laboratories for studying the properties of DM on small scales. Dwarf galaxies provide significant insight into the early stages of galaxy formation and evolution, and due to their sizes and inability to self-regulate, these structures are easily disrupted and can serve as tracers of galaxy assembly over cosmic time. The small-scale structure challenges within the ΛCDM framework are actively researched through the study of dwarf galaxies and show promise to address discrepancies between theory and observation.

2.2. Classification of Dwarf Galaxies

Dwarf galaxies, like their galactic-scale counterparts, are diverse in type and classified by morphological properties. These DM dominated systems differ significantly in their physical, observable characteristics and treatment in simulations. In terms of stellar populations, dwarf galaxies are typically comprised of older stars that formed early in the history of the Universe and contain some of the most metal-poor stars in nature. However, there is evidence of recent star formation in some dwarfs (Weisz et al., 2014), indicating that these small structures have diverse SFHs.

Dwarf galaxies are commonly divided by whether or not star formation is still ongoing. Dwarf galaxies that no longer have gas available to form stars are labeled as dwarf spheroidal (dSphs) and typically found as satellites to Milky-Way like galaxies. dSphs are small and faint with older stellar populations (Tolstoy et al., 2009). Dwarf galaxies with gas and ongoing star formation are known as dwarf irregulars (dIrrs) and are generally not found as satellites to larger galaxies, or otherwise known as field galaxies. As such, dIrr galaxies are typically found in isolated environments away from large galaxies and galaxy clusters. In similarly isolated environments, Blue compact dwarf galaxies (BCDs) are also gas-rich and exhibit intense star formation with a host of young, massive stars.

As discussed in Chapter 1, the small-scale mass regime relevant for addressing ΛCDM challenges has stellar masses less than 10^{11} $M_{\odot}$. For this work specifically, "dwarfs" refer to galaxies with $M_{*} \lesssim 10^{9}$ $M_{\odot}$ and are classified according to mass following the prescription outlined by Bullock & Boylan-Kolchin (2017) and in accordance with Lazar et al. (2020): bright dwarfs ($M_{*} \approx 10^{7-9}$ $M_{\odot}$), classical dwarfs ($M_{*} \approx 10^{5-7}$ $M_{\odot}$), and ultra-faint dwarfs (UFDs, $M_{*} \approx 10^{2-5}$ $M_{\odot}$).

2.2.1. Bright Dwarfs

The bright dwarf mass range is considered the limit for field galaxy surveys to detect faint galaxies. Traditionally, galaxies fainter than absolute magnitude of $M_V = -15$ or -16 are considered dwarf galaxies (Hodge, 1971; Tammann, 1980) with the brightest dwarfs having absolute magnitudes around $M_B = -18$. Bright dwarfs are more luminous and often have ongoing or recent star formation as they are typically dIrrs located in field environments where they are relatively isolated and gas is accessible to maintain active star formation (Mateo, 1998; Tolstoy et al., 2009).

As a result, bright dwarfs have diverse stellar populations having undergone extended SFHs. These dwarfs host mixed stellar populations of young, metal-rich stars and older, metal-poor stars that formed at varying epochs (Koposov et al., 2008). An example of this can be seen in dIrrs that show evidence of ongoing star formation and host a vast range of stellar populations (Mateo, 1998; Tolstoy et al., 2009). This supports the fact that bright dwarfs often have significant amounts of gas at some point during their formation or are otherwise gas-rich for extended star formation. Bright dwarfs can also have multiple bursts of star formation over billions of years, leading to bursty SFHs in some dwarfs that have only recently stopped forming stars (Tolstoy et al., 2009), as will be shown in Chapter 5.

Bright dwarfs can however belong to galaxy groups or clusters. An example of this is the Large Magellanic Cloud (LMC) which is a bright dwarf galaxy and satellite of the MW. The LMC is a dIrr with regions of active star formation and diverse stellar populations. The LMC is part of the Local Group — a collection of galaxies including the MW, M31, and several smaller galaxies that are studied to understand the formation and evolution of galaxies as well as DM properties. Due to its proximity and hosting numerous dwarf galaxies, the Local Group is a key environment for studying the dynamics of these galaxies, determining the distribution of DM, and testing models of DM halo formation.

Observations of bright dwarf galaxies and their DM structure provide important constraints on galaxy formation models under the ΛCDM model, as the bright dwarf mass regime is significant enough to allow for reliable measurements of DM content through stellar kinematics. Galaxies that have rotating disks allow for direct velocity measurements of stars and gas from the Doppler shift of spectral lines, which can then be used to infer the mass contribution from DM. In the case of bright dwarfs, these systems often have gas disks extending far enough out to allow for velocity measurements of the rotation curve using Equation 1.8 to infer DM properties such as mass and the density profile outlined in Section 1.2. In fact, recent studies simulating the reconstruction of rotation curves show that bright dwarf galaxies with thin, ordered, extended disks reproduce accurate circular velocities within a ten percent error (Sands et al., 2024), allowing for consistent interpretations of the DM content in this mass regime.

2.2.2. Classical Dwarfs

Prior to deep sky surveys such as the Sloan Digital Sky Survey (SDSS), classical dwarfs were considered the faintest galaxies found in nature. In the classical regime, dwarfs have stellar masses between 10^5 $M_\odot$ and 10^7 $M_\odot$ (Koposov et al., 2008) and are fainter than $M_V = -14$. Classical dwarfs are older, less luminous galaxies but are still generally easy to observe and have been detected and studied since the early 20th century (Mateo, 1998).

Classical dwarfs have established stellar populations and are typically dSph satellites of larger galaxies that consequently influence the dynamics and evolution of these systems. The interactions between classical dwarfs and the host galaxy may have quenched star formation billions of years ago. As a result, classical dwarfs typically exhibit little to no ongoing star formation, and are likely gas-poor due to environmental processes and tidal interactions from the influence of their host galaxies, as these interactions remove the gas over time. Classical dwarf galaxies, particularly dSphs in the Local Group, are therefore used to study galactic evolution, DM content, and SFHs in low-mass, gas-poor systems. Due to the ages of their stellar populations, classical dwarfs provide insight about the early formation of stars in the Universe.

As discussed in the previous subsection, kinematic measures on the scale of dwarf galaxies require that DM properties must be inferred. As dSphs lack rotating gas and stellar components that would make rotation curve measurements possible, typical classical dwarf galaxy DM properties and density profiles must be inferred some other way. Galaxies without rotationally supported disks are instead dependent on the distribution of individual stellar velocities, or the stellar dispersion, rather than the rotation of the disk. In contrast with systems that can be directly measured and use the virial theorem to determine mass content, the mass estimates of dispersion-supported galaxies are determined using a half-light radius, or the radius at which half of a galaxy's light is emitted. Wolf et al. (2010) accurately determined DM halo masses of observed MW satellites by estimating masses relative to the half-light radius

$$M_{1/2} \propto (\frac{\sigma}{km\ s^{-1}})^2\,(\frac{R_{1/2}}{pc})\,M_{\odot}, \tag{2.1}$$

where σ is the velocity dispersion and $R_{1/2}$ is the projected two-dimensional half-light radius and is routinely used to estimate the masses of dispersion-supported systems under the ΛCDM framework.

2.2.3. Ultra-Faint Dwarfs

With the advent of deep sky surveys such as SDSS and the Hubble Space Telescope (HST), even smaller and fainter dwarf galaxies with low luminosities and stellar masses have been discovered in regions of space surrounding the MW and M31. UFDs range from 10^2 $M_{\odot}$ to 10^5 $M_{\odot}$ and have absolute magnitudes fainter than approximately $M_v = -8$ as a result of having significantly fewer stars than bright and classical dwarfs (Brown et al., 2014; Simon & Geha, 2007; Simon, 2019). This makes UFDs unique in that their mass-to-light ratio is on the order of several hundred to one thousand and serve as the most DM-dominated systems in the Universe . Although UFDs are not strictly distinct from the physical properties governing more luminous dwarfs, it has become necessary to label them differently as they are extremely DM dominated and presumably represent the extreme end of the distribution of galaxy properties for having the smallest stellar masses, lowest surface brightness, smallest sizes, oldest ages, and the simplest SFHs (Simon, 2019).

In addition, these dwarfs have unique SFHs that span the cosmic timescale, having formed early in the history of the Universe. UFD stellar populations are predominately comprised of Population II stars that are metal-poor and over 10 billion years old, and these systems no longer experience active star formation. In fact, UFDs are likely to only have minimal, brief episodes of early star formation. In contrast with virtually all larger systems, UFDs experience quenched star formation before or during the reionization epoch 1-2 billion years after the Big Bang (Brown et al., 2014) and experienced little to no further evolution after that time. As a result, UFDs are considered relics of the early Universe and provide unique insight into the conditions present when galaxies first started forming (Simon, 2019).

As UFDs are the most DM-dominated systems known, the difficulty in detecting them means that only the brightest of these systems will be observed beyond the Local Group in the future. Additional constraints on UFD characterization will likely be limited to satellites of the MW, and these systems most closely resemble previously-known dSphs in the Local Group (Simon, 2019). As such, UFDs follow the same velocity dispersion prescription for DM measurements outlined in Section 2.2.2 and Equation 2.1. It is also worth noting that the baryonic components in these systems are likely to have little impact on their dynamics and evolution process. Unlike bright and classical dwarfs, the inefficiency of their SFHs suggests that influence from feedback processes should be negligible and do not alter the internal density structure (Brooks & Zolotov, 2014a; Di Cintio et al., 2014; Oñorbe et al., 2015). The unique SFHs of UFDs makes them an important piece of modern galaxy evolution and understanding the DM response in low mass halos. The impact of these implications will be shown in Section 5.2.

2.3. Challenges to ΛCDM

As discussed in Chapter 4, the measurements of galaxy rotation curves revealed physical evidence for DM and ushered in a new cosmological frontier. The ΛCDM paradigm, along with other DM frameworks, emerged to explain key observational measurements of cosmic acceleration, studies of the CMB, and the clustering of large-scale structures. After the first N-body simulation resolved the internal structure of CDM halos on small-scales (Dubinski & Carlberg, 1991), several challenges to the CDM framework emerged as observational data was found in conflict with models that only accounted for DM. In this section, the three most prominent challenges in the current literature — the missing satellite problem, the cusp-core problem, and the too-big-to-fail problem are discussed first to address fundamental predictions about DM and the hierarchical nature of structure formation under the ΛCDM model. Additional tensions such as the M_*-M_{halo} relation, the diversity of dwarf sizes and rotation curves, and satellite planes are discussed for a complete overview of the current state of ΛCDM tensions with observations of dwarf galaxies.

2.3.1. Missing Satellites Problem

The ΛCDM model predicts a DM dominated Universe in which a hierarchical structure emerges. Under this paradigm, CDM clumps together under gravity to serve as the foundation for larger structures to form. These clumps of DM attract cooled gas, eventually forming stars and satellite galaxies at the sites of DM subhalos. Following this prescription, smaller DM halos also collapse earlier than larger ones and have sufficient molecular cooling within the gas to form galaxies. Consequently, smaller galaxies collapse earlier, indicating that satellites of the MW likely formed long before the host galaxy was fully assembled, or in other words, had a chance to disrupt the evolution and population of its satellites. As a result, MW-like galaxies should have thousands of DM clumps with a satellite population that is proportional to this number.

Despite efforts to understand satellite abundance in the Local Group, the predicted number of DM subhalos is inconsistent with the number of observed satellites as DM-only simulations of MW-mass halos predict significantly more of these DM subhalos than observed dwarf galaxies around the MW or M31 (Klypin et al., 1999; Bullock et al., 2000; Brooks et al., 2013; Simon, 2019). Bullock & Boylan-Kolchin (2017) determined that DM subhalos with masses on the order of 10^7 $M_\odot$ or greater should have sufficient mass to support the molecular cooling required to form visible satellites, and until recently, the number of satellites within the virial radius of the MW was approximately 50 — a factor of five less than expected (Simon, 2019).

It is likely that detectors have historically been limited in the discovery of satellites, particularly for UFDs. A recent search for MW satellites using the HSC-Subaru Strategic Program (HSC-SSP) found two new satellites (for a total of 9 satellites), which resulted in a much higher discovery rate than expected from the most recent ΛCDM model predictions (Homma et al., 2024). The continuous discovery of UFDs and predicted increase in this number with future surveys such as the Rubin Observatory's large-scale photometric survey (LSST) will likely eliminate the missing satellites problem altogether.

2.3.2. Cusp-Core Problem

Following the inner density prescription outlined in Section 1.2.1, CDM simulations robustly predict DM halos to have cuspy density profiles that rise steeply near the center:

$$\rho(r) \propto r^{-\gamma} \tag{2.2}$$

with $\gamma \approx 1$ for the inner radii of small galaxies (Governato et al., 2010a). However, observations show a wide diversity of rotation curves in low surface brightness galaxies, with curves typically rising more slowly from the center before declining in the outer regions (de Blok et al., 2001). In fact, many DM-dominated galaxies in the lower mass regime show measured rotation curves that fit with constant-density cores where $\gamma \approx 0$ (Simon et al., 2005; de Blok et al., 2008), indicating that low-mass galaxies are better defined by cored DM density profiles and deviate from the predicted NFW profile under ΛCDM. This tension is known as the cusp-core problem.

This slow rise also suggests that DM is not as centrally clustered at the center as predicted by ΛCDM simulations. While the cusp-core problem argues the curvature of the density profile, another issue arises in that the total amount of DM in the central regions of satellites and UFDs where the total amount of DM is over-predicted by simulations regardless of whether or not a cored profile is assumed (Oman et al., 2015). This suggests that ΛCDM halos are both too dense and too cuspy to agree with observations and likely point to a common issue with feedback effects in the central regions or disruption from environmental effects. The over-dense central regions may also be linked to the too-big-to-fail problem in the following subsection, where predictions of the number of the most massive (dense) subhalos is significantly higher than the number of observed satellite galaxies that should be able to form within them.

CDM simulations generally predict uniform rotational behavior and are unable to account for the diversity of rotation curves in small galaxies, which will be further discussed in Section 2.3.5, or why DM halos diverge from observed density profile slopes and central region density without additional considerations. It becomes important to consider whether the properties of DM need modification or if additional physical processes are involved — particularly baryonic processes that can affect DM distributions (Pontzen & Governato, 2012). As a result, current research aims to understand the impact of baryonic feedback processes on the DM response or otherwise search for alternative DM models to explain the observed properties of small galaxies.

2.3.3. Too-Big-to-Fail Problem

As discussed in Section 2.2, the DM mass of dwarfs are indirectly determined by using the stellar kinematics of stars within the half-light radius. Using this approach, the central masses of MW satellites should be consistent with subhalo masses using CDM simulations of MW-mass halos, or in other words, the most massive subhalos should be able to form satellites. Instead, a study by Springel et al. (2008) revealed much smaller DM masses for the most massive MW satellites, indicating that the subhalos were too centrally dense to host the MW satellites. This result was counter-intuitive, as DM subhalos on these scales are massive enough to theoretically host these galaxies, or should be 'too-big-to-fail' at hosting galaxies.

Observational evidence shows that these subhalos generally lack luminous satellite galaxies despite the fact their gravitational potentials wells are deep enough to retain and cool gas to form stars (Boylan-Kolchin et al., 2011). In addition to the tension with satellites, other field galaxies in the Local Group (Garrison-Kimmel et al., 2014) and otherwise isolated dwarfs outside of the virial radius of the MW were found to exhibit the same issue, solidifying the too-big-to-fail problem as a challenge to the ΛCDM model. This again is indicative that some physical process or limitation is unaccounted for within the ΛCDM framework. These may include baryonic feedback processes that quench star formation, detector limitations, or the properties of DM itself (Brooks & Zolotov, 2014b).

2.3.4. M_*-M_{halo} Relation

The stellar-to-halo mass relation (SMHM) is used to relate the total DM halo mass to the amount of stellar mass to understand how efficiently dwarf galaxies form and evolve in the context of star formation. As dwarf galaxies are DM-dominated, the stellar mass of dwarf galaxies is significantly lower than the mass of the DM halo. This also suggests that dwarf galaxies experience inefficient star formation, likely due to feedback processes and outflows that can eject star-forming gas and reduce the total halo mass, or otherwise experience environmental effects. As a result, any attempts to link simulated halos to the number of observed galaxies using this relation becomes exceeding difficult for ultra-faints and low-mass galaxies with significantly lower stellar mass. In addition, Munshi et al. (2019) find that the SMHM relation for UFDs varies with the star formation prescription that is implemented, indicating that the SMHM relation is highly dependent on the simulation model and choice of subgrid physics.

Furthermore, as discussed in Section 2.2, the inferred masses of DM halos are dependent on whether the system is rotationally supported or dispersion-supported. For UFDs that use individual stellar velocity dispersions, measurements of the halo mass are likely to introduce further uncertainties, rendering to the SMHM relation even more challenging. In addition, halo mass also varies depending on prescription used for defining the inner radius as outlined in Section 2.2.2 or Equation 1.7, further complicating any comparisons between models and observation.

2.3.5. Dwarf Galaxy Sizes and Rotation Curves

Under the ΛCDM framework, DM halos — the sites of galaxy formation — are expected to predict a reasonably uniform range of galactic structures and galaxy sizes. As discussed previously, the feedback that occurs as a result of bursty star formation can alter the gravitation potential of these systems and reduce the central DM density of halos. As described in Section 2.2, the majority of classical and ultra-faint dwarfs are dispersion-supported systems due to their DM content and exhibit cored DM profiles. It would be reasonable to assume that dwarf galaxy sizes are directly related to their DM halo mass, however, simulations of low-mass galaxies that link star formation to regions of high density gas and predict fluctuating bursts of star formation (Stinson et al., 2006; Di Cintio et al., 2014; Sparre et al., 2017) show a wide diversity of sizes regardless of fixed mass.

The most extreme cases of low-surface brightness, or diffuse galaxies, and extremely bright compact dwarfs that are stripped of DM are difficult to account for in simulations. Under the ΛCDM model, dwarf galaxies are sensitive to feedback process that suppress star formation and expected to have lower stellar masses. As such, the existence of compact dwarfs are difficult to explain without addressing the physical processes such as star formation efficiencies and galaxy threshing (Bekki et al., 2003) where strong tidal fields of nearby clusters remove the outer components of dwarfs. Applebaum et al. (2021) were able to reproduce observed galaxy sizes with the DCJL simulations that ranged from diffuse to compact galaxies, but only found one ultra-compact dwarf (UCD) among the sample, confirming that the most extreme example of a compact dwarf was an isolated case. In contrast, ultra-diffuse galaxies (UDGs) and some UFDs are larger than expected from their inferred halo masses, further contributing to the issue with size diversity. Sales et al. (2022) finds that Local Volume dwarfs are significantly more numerous than those predicted by high-resolution simulations of dwarf galaxies, indicating that strong feedback may also contribute to the diversity problem with dwarf sizes.

In addition to dwarf galaxy sizes, tension is also introduced with the diversity of rotation curves. As discussed in Section 2.3.2, baryonic feedback is capable of producing DM cores in bright and some classical dwarfs and Section 2.2 discusses how DM distributions in dwarf galaxies typically favor cored density profiles. However, observations reveal that dwarf galaxies of similar masses have varying rotation curves, with some dwarf galaxies following the NFW profile or showing even cuspier profiles than predicted by NFW models (Oman et al., 2015; Relatores et al., 2019). Reproducing the diversity of these rotation curves is a significant challenge to ΛCDM model, as existing models struggle to reproduce the observed diversity in rotation curves consistently with the expected properties of these galaxies. Furthermore, Oman et al. (2016) posit that the diversity of rotation curves is due to an 'inner mass deficit' rather than conflicting density profiles, suggesting that simulations currently fail to accurately model the diversity of baryonic effects in the central regions of dwarf galaxies. As such, future observations will be crucial for providing constraints on dwarf galaxy rotation curves and the distribution of DM.

2.3.6. Satellite Planes

When considering how dwarf galaxies are distributed around larger host galaxies such as the MW and M31, the arrangement of satellites introduces another challenge to the ΛCDM model. Assuming that nature is hierarchical, satellites are expected to be randomly distributed around their hosts with orbits that do not necessarily resemble a coherent pattern or direction. Pawlowski & Kroupa (2020) recently compared proper motion measurements of 11 classical satellites of the MW to assess tensions with ΛCDM predictions, and found that the orbital motions were correlated in planes perpendicular to the MW. Previous studies by McConnachie & Irwin (2006) found that satellites of M31 also exist within a flattened, coherent structure and were later revealed to exhibit correlated kinematic motion along their satellite plane by Sohn et al. (2020). In addition, Müller et al. (2021) found that the vast majority of dwarf galaxies in the nearby Centaurus A group (Cen A) showed coherent motion from their measured line-of-sight velocities, confirming that tensions with the arrangement and kinematics of satellites extend beyond the Local Group.

Comparing observations to simulations further complicates the problem with satellite planes. When comparing the updated Gaia DR2 proper motions to both a hydrodynamical simulation and a DM-only counterpart, Pawlowski & Kroupa (2020) found that both simulations produced identical results and were unable to reproduce the expected orbital correlation of satellites, indicating that the baryonic physics in hydrodynamical simulations could not alleviate the problem. Müller et al. (2021) found similar results, with only 0.2 percent of Cen A analogs in both hydrodynamical and DM-only simulations showing satellites that move in flattened, coherent planes. In contrast with other ΛCDM challenges that can be alleviated with baryonic physics, the motion and distribution of satellites remains inconsistent between observations and simulations and proves to have be one of the strongest tensions.

2.4. Solutions to ΛCDM Challenges

These challenges to ΛCDM all point to similar proposed solutions that either require moving beyond DM-only simulations to incorporate baryonic physics or modifications to the ΛCDM model using alternative DM models. Baryonic feedback from physical processes such as SN events and subsequent SN-driven outflows redistribute matter in galaxies, shaping many fundamental properties of small galaxy formation and evolution. Alternative DM models are used to address the particle nature of DM and how viable DM candidates impact structure formation. These solutions are tested in simulations and compared to observations to make the ΛCDM framework successful across all relevant scales.

The solutions discussed in the following section are divided as follows: solutions that exist within the current framework of ΛCDM in the form of baryonic feedback and serves as the foundation for the work presented in the following chapters, and solutions that require modifications to model itself in the form of alternative DM models to provide a complete discussion of on the current state of solutions to ΛCDM challenges.

2.4.1. Alternative Dark Matter Models

The ΛCDM framework has remained at the forefront of successfully explaining the evolution of the Universe, and with the advent of DM becoming a prominent component of cosmological modeling, the connection to particle physics has become an important avenue to address ΛCDM challenges as cosmologists must make assumptions about the origins and particle nature of DM. Alternative DM models serve as theoretical frameworks to address these challenges. Understanding DM remains a key challenge in cosmology, with significant implications for both particle physics and understanding cosmological structures within the ΛCDM model.

As described in Section 1.1.1, density perturbations as a result of cosmic inflation seeded the growth of structure formation. The particle nature and properties of various DM models affect the cosmological power spectrum differently. In particular, DM models are differentiated by their "free-streaming length" (Boyarsky et al., 2009; Bertschinger, 2006), which defines how far particles travel before density perturbations grow significantly and signifies a cut-off scale from the linear spectrum where particles fall into potential wells. As such, particles with a longer streaming lengths are able to travel further distances and therefore smooth density perturbations on larger scales and DM models are determined based on their relative impact on structure formation.

As discussed previously, CDM structure formation is hierarchical in which small scales collapse and merge to form larger structures. CDM particles are typically assumed around $m \sim 100$ GeV which allows these massive particles to remain cold and non-relativistic throughout cosmic history. As such, CDM has a negligible thermal velocity and a free-streaming length on the order of $\leq$ pc that supports a power spectrum in which the accretion and merging of smaller scales is plausible and does not hinder structure formation at any relevant scale (Boyanovsky, 2021). Weakly Interacting Massive Particles (WIMPS) are a favored DM particle candidate for maintaining thermal equilibrium in the early Universe and having a relic density that matches observed DM densities (Feng & Kumar, 2008). Attempts to detect WIMPs over the past several decades have yet to provide evidence of these particles, leading to alternative paradigms to address the challenges of ΛCDM on small scales (Cushman et al., 2013).

2.4.1.1. Warm Dark Matter

In the approach to alter predictions for CDM models, Warm Dark Matter (WDM) models result in the suppression of density perturbations on larger scales. WDM models assume that DM particles have semi-relativistic velocities that make the particles "warm" relative to their CDM counterparts. Having higher thermal velocities in the early Universe, WDM particles are assumed to have masses on the order of $m \sim 1$ keV and have free-streaming lengths on the order of a few kpc, allowing them to preserve small-scale density fluctuations and potentially suppress the formation of higher-mass DM halos. Leading WDM candidates such as sterile neutrinos (Dodelson & Widrow, 1994) are able to produce DM cores (Boyanovsky, 2021), while special cases of axions (Kim & Carosi, 2010) exhibit WDM-like behavior (Fuzzy DM) that can suppress structure formation on small scales (Niemeyer, 2020). Furthermore, the impact of suppressed structure formation extends beyond the number of DM halos. Since cosmological structures grow in a hierarchical manner, Bullock & Boylan-Kolchin (2017) discuss that the suppression of small perturbations delays the formation of halos and that models with a power spectrum favoring smaller scales leads to halos with weaker central gravitational potentials that depend on the density of the Universe when they formed.

Despite the potential successes of a WDM model, it is inconsistent with observations of hydrogen absorption lines in observed dwarf galaxies (Schneider et al., 2014). The Lyman-Alpha forest series of absorption lines provides a detailed map of the distribution of matter in the early Universe and constrains the free-streaming length of WDM particles. This ultimately limits the mass and temperature these particles can be, as too light and warm results in a suppression of smaller structures that is inconsistent with observations of the Lyman-Alpha series (Viel et al., 2005; Boyarsky et al., 2009). This inevitably influences galaxy formation by delaying the merging process required to form larger galactic structures. Observations of high redshift galaxies show that dwarf galaxies are already present, and form early on in the history of the Universe (Viel et al., 2013).

Perhaps most importantly, it is unclear if there are significant differences between WDM models and CDM models that incorporate baryonic feedback processes. Like CDM, WDM models can successfully produce density profiles in small-scale DM halos that are smoother and more cored by suppressing structure formation. Governato et al. (2015) find that both CDM and WDM baryonic simulations of faint dwarfs independently produce similar lower central densities and flatter DM profiles that are consistent with observations of field dwarf masses, indicating that SF criteria and feedback processes drive the production of realistic DM distributions regardless of DM model.

2.4.1.2. Self-Interacting Dark Matter

As described in Section 1.1.1, CDM particles only interact through gravity, but these interactions are most significant between DM particles and the large-scale gravitational potential rather than between individual particles (Bullock & Boylan-Kolchin, 2017). In contrast with CDM and WDM models that are effectively collisionless, DM self-interactions, or Self-Interacting DM (SIDM) (Spergel & Steinhardt, 2000) models include non-gravitational interactions between DM particles. As SIDM models focus on self-interactions, the free-streaming length becomes negligible and CDM-like behavior is still expected on large scales. Instead, SIDM incorporates an interaction cross-section (σ) which is often expressed in terms of density and particle mass as σ/m, where σ is an effective area in which interactions occur and m is the mass of the particle.

Spergel & Steinhardt (2000) proposed an analytically derived SIDM cross-section to address tensions with central densities of DM halos, and found that σ/m $0.1 - 100\text{cm}^2\text{gm}^{-1}$ would produce DM cores. Further studies by Rocha et al. (2013) using new SIDM N-body simulations found that $\sigma/m = 1\text{cm}^2\text{gm}^{-1}$ models were unable to match halo core densities to observations of galaxy clusters, low surface brightness spirals (LSBs) and dSphs, but a value of $\sigma/m = 0.1\text{cm}^2\text{gm}^{-1}$ was able to reproduce observed core sizes and central densities for the same structures. More recently, Cruz et al. (2021) found that SIDM interactions with a cross-section value of $\sigma/m = 1\text{cm}^2\text{gm}^{-1}$ suppressed DM in the central regions of MW-like galaxies, resulting in a mass deficit and lower gas density relative to CDM and a higher production of SF. In addition, a recent study by Rose et al. (2022) using SIDM and hydrodynamical simulations to investigate the interactions of SIDM and baryons found agreement between the two models for dwarf galaxy mass scales, indicating that SIDM was a strong candidate to address the cusp-core and too-big-to-fail problems.

However, the success of SIDM is largely dependent on the cross-section of self-interaction. Interactions between DM particles will need to be able to preserve the behavior of CDM on large scales, while being flexible enough to produce a cross-section that is successful across scales between dwarf galaxies and galaxy clusters. Eckert et al. (2022) conclude that a velocity-dependent cross-section can be consistent with SIDM constraints derived from galaxy clusters while still solving the cusp-core problem in dwarf galaxies. In addition, Fry et al. (2015) find that CDM and SIDM simulations incorporating baryonic feedback show similar observational signatures for larger halo masses, but conclude that despite implementing a larger cross-section value, SIDM becomes negligible for halos on the order of $< 10^6$ $\text{M}_\odot$ and will require a velocity-dependent cross-section to produce DM cores. The successes of these results, particularly when feedback is introduced to influence the distribution of DM, show that SIDM is a viable DM model to address tensions with the cusp-core and central density problems without altering the behavior CDM on large scales.

2.4.2. Baryonic Processes

Although alternative DM models are successful in some aspects for small-scale structures, there is no single model that is able to resolve all of the discrepancies between theory and observation. In fact, these models may still require additional physical processes to be completely successful. The most significant process that aids both alternative DM models as well as ΛCDM challenges is baryonic feedback — the impact of ordinary matter from SNe, gas, stars and radiation. These processes have crucial roles in shaping the structure of galaxies, regulating star formation, and affecting the distribution of DM.

To reconcile the predictions and observations of satellite abundance, there are several possible solutions. Klypin et al. (1999) suggest that discarding the possibility that $\approx 80\%$ of the Local Group satellites have been missed in observations, the discrepancy may be explained by identifying an overabundance of DM satellites in the Local Group or physical baryonic processes from SNe-driven winds during the early galaxy formation, indicating the importance of baryonic processes on these mass scales from UV feedback and suppressed gas accretion. In fact, current ΛCDM simulations that incorporate baryonic physics are shown to be consistent with the observed number of satellites around the MW and M31 (Sawala et al., 2016; Wetzel et al., 2016; Munshi et al., 2021), suggesting that it is possible to resolve the missing satellites problem for bright and classical dwarf mass regimes.

Simulations that incorporate baryonic feedback have been shown to produce core-like density profiles. This is achieved by incorporating subgrid baryonic physics in hydrodynamic simulations, which will be discussed in detail in Chapter 3. The implementation of baryonic feedback is shown to remove central cusps in dwarf galaxies and successfully predict cored profiles (Navarro et al., 1996; Pontzen & Governato, 2012; Chan et al., 2015), as an approach to resolve the cusp-core problem. In essence, galaxies need to form enough stars to produce energy from SNe events to redistribute DM and create cores. This indicates that core formation is dependent on the mass of formed stars, and will be sensitive to the fraction of baryons used for star formation prescriptions, as will be highlighted in Section 4.2.

Subgrid models of SN feedback drive baryonic matter from the center of CDM halos, causing fluctuations in the gravitational potential and lowering the central density of dark matter (Governato et al., 2012; Zolotov et al., 2012; Di Cintio et al., 2014; Read et al., 2016). The importance of SN-driven outflows on the central DM structure of dwarfs have already been shown (Navarro et al., 1996), but it has recently become important to understand that star formation over extended periods of time can drive gravitational potential fluctuations to produce cores. These fluctuations in the central gravitational potential indicate that both a supply of cold gas undergoing collapse and rapid expansion may be necessary to produce cored halos (Pontzen & Governato, 2012).

The impact of baryonic feedback on core formation can be determined by comparing the inner slopes of DM halos measured at $1-2\%$ of the virial halo radius as a function of M_*/M_{vir} (denoted as M_*/M_{halo} in the following chapters of this work) and discussed in detail in Chapter 5. Numerous studies find that core formation for baryonic simulations is most efficient at $M_*/M_{halo} \approx 0.005$, corresponding to bright dwarfs on the order of $M_* \simeq 10^{8-9}$ $M_\odot$ (Di Cintio et al., 2014; Chan et al., 2015; Tollet et al., 2016; Lazar et al., 2020). The baryonic feedback introduced in this work and the results of formed and sustained DM cores for dwarf galaxies will be discussed in Chapter 5.

As stellar feedback from SN events has the potential to produce cores, it would be logical to conclude that approximately half of the MW's classical dwarfs above $M_* \approx 10^6$ $M_\odot$ have low central densities due to the abundance of star formation. However, the other half of these systems also have to low central masses and need to be explained by other feedback mechanisms. MW satellites experience other types of feedback such as tidal stripping, ram pressure stripping, and other forms of environmental feedback from the gravitational potential of the MW that can lower the central densities of these systems (Zolotov et al., 2012; Brooks & Zolotov, 2014a; Brook & Di Cintio, 2015; Sawala et al., 2016; Wetzel et al., 2016). These effects are difficult to resolve accurately with the current state of hydrodynamic simulation resolution, but necessitate that environmental factors systematically differ for satellite and field galaxies.

The implementation of baryons provides several solutions, as high-resolution hydrodynamical simulations produce feedback-induced cores, particularly for mass ranges corresponding to bright and classical dwarfs where core formation is the most efficient. Below this threshold, environmental effects are needed to address the too-big-to-fail problem for satellite galaxies and becomes significantly important to explain the central densities of the lowest-mass dwarf galaxies. Additionally, baryonic simulations produce lower halo and subhalo masses than DM-only simulations as a result of stellar feedback removing significant amounts of baryons from, regardless of whether or not they produce DM cores (Brooks & Zolotov, 2014a; Sawala et al., 2013), indicating that future observations from the Rubin and VRO surveys will be necessary to fully understand the cusp-core problem and too-big-to-fail problem for field dwarfs that are unaffected by environmental feedback.

2.5. Conclusion

In summary, dwarf galaxies offer unique insights into the behavior of DM and the processes governing galaxy formation on small scales. By exploring their classifications and the challenges they present to the ΛCDM model, this chapter has highlighted their significance in resolving key cosmological issues. However, understanding these galaxies fully requires sophisticated modeling techniques that go beyond DM-only simulations. Chapter 3 will explore the various simulation methods used to study dwarf galaxies and focus on the significance of integrating baryonic physics to address current theoretical challenges.

CHAPTER 3

Simulations

3.1. N-Body Simulations

To model physical processes, N-body simulations are used to understand the formation and evolution of cosmic structures. These computational simulations model the gravitational interactions of a set number of N particles that represent a mass. Depending on the scale of the simulation, the particles can represent individual DM particles, ordinary matter such as gas and stars, or even individual galaxies. N-body simulations are used to study the dynamics of large galactic structures by tracking the gravitational interactions of these particles over time, as each particle obeys Newtonian equations of motion and is subject to the gravitational forces exerted by all particles in the system.

N-body simulations incorporate discrete time steps to iteratively update the positions and velocities of all particles in the system as they gravitationally interact. As each particle interacts with all others in the system, calculations at each time step are demanding in both computation time and resources that ultimately limit the number of particles that can be simulated. Cosmological simulations therefore model particles that represent massive clumps of DM or baryonic matter such as stars rather than individual mass particles. Since simulation resolution is finite, studies are typically dependent on a specific scientific goal. High-resolution simulations on smaller scales can describe the detailed structure of galaxies, the behavior of stars within galaxies, and resolve other small-scale phenomena, whereas lower-resolution simulations can provide information about the evolution of large scale structures on massive scales that extend to the entire observable Universe.

3.1.1. DM-Only Simulations

In applications to ΛCDM, a particular class of N-body simulations models the behavior and dynamics of DM (without the effects of baryonic matter) to understand the evolution and distribution of DM on massive scales. DM clumps together under gravitational forces and shapes the filaments, clusters, and voids of the cosmic web and dominates the gravitational potential wells of galaxies and galaxy clusters. As a result, DM-only simulations reveal important properties such as the mass distribution, density profiles, and substructure of DM halos and how these cosmic structures form within them. Furthermore, populations of satellite galaxies are predicted by DM-only simulations to form within the subhalos of larger DM halos. As such, these simulations are useful to understand the nature of DM halos, subhalos, and how DM influences structure formation under the ΛCDM framework.

While DM-only simulations are key to understanding the distribution of DM on large scales, they do not realistically model visible structures and face challenges when trying to match observational data. It is necessary to implement baryonic physics into simulations for them to form galaxies, and these processes also impact key properties such as density profiles and rotation curves. SN feedback, gas cooling, and star formation significantly alter the evolution of galaxies and clusters to form the structures observed today. Galaxies form as a result of gas cooling and condensing, and the interactions of gas and DM influence the mass distribution and dynamics of DM halos. Additionally, the injection of energy from SNe and other star formation processes can significantly alter the central regions of halos, leading to inaccurate density profiles for simulations that do not incorporate baryonic physics.

3.2. Hydrodynamic Simulations

Galaxies form as a result of the cosmological growth of density fluctuations, which is a highly nonlinear process that is impossible to treat analytically. To address the limitations of DM-only simulations, hydrodynamic simulations incorporate both DM and baryonic matter from stars, gas, and radiation to model the complex feedback interactions that shape large, visible structures. Unlike DM-only simulations that only account for gravitational interactions of DM particles, hydrodynamic simulations incorporate processes of gas dynamics, gas cooling, SN feedback, black hole (BH) accretion, and star formation to model the formation and evolution of galaxies (Somerville & Davé, 2015). Hydrodynamics — the physics of fluids — is implemented to simulate the behavior of gas and reveal how gas interacts with DM in galaxies, galaxy clusters, the intergalactic medium (IGM) and ISM, and forms stars.

As discussed in Section 3.1.1, the gravitational potential wells of DM serve as the foundation for which gas collapses, forms stars, and ultimately evolves into a galaxy. In hydrodynamic simulations, DM is typically modeled as particles that influence the gravitational potential and drive large-scale structure formation. Baryons are modeled as fluid — a dense set of particles treated as a continuous flow under the influence of gravity and cosmic expansion. As such, hydrodynamic simulations model the motion of fluid as an ideal gas by using a fundamental set of partial differential equations to obey the conservation of mass, momentum, and energy (Somerville & Davé, 2015). These are known as Euler equations, a form of the Navier-Stokes equations that assume no conduction or forces from internal friction — otherwise known as a fluid's viscosity or "resistance to flow." In most cases, however, it is necessary to add an artificial viscosity term to hydrodynamical codes in order to handle convergent flows and shocks (Somerville & Davé, 2015).

3.2.1. Hydrodynamic Equations

Hydrodynamic simulations incorporate equations of motion for particles to represent the behavior of gas dynamics, where properties such as mass, energy, and momentum are conserved (Springel, 2010). Mass conservation is represented by the continuity equation, which in proper coordinates (r, t) where the coordinate system is fixed in time, is given by

$$\frac{\partial \rho}{\partial t} + \rho \nabla \cdot \mathbf{v} = 0, \tag{3.1}$$

where ρ is the fluid density, t is time, and **v** is the flow velocity vector field (Peebles, 1980b). This equation states that the rate at which mass enters and leaves a system is equal by incorporating a time derivative to account for the accumulation or loss of mass and a divergence term to represent the difference in flow upon entering and leaving the system. As the Universe is expanding, the continuity equation may be converted to a co-moving coordinate system with a co-moving spatial coordinate x, where $r = a(t)x$ is the proper position and $a(t)$ is the cosmic scale factor:

$$\frac{\partial \rho}{\partial t} = -\frac{1}{a^2} \rho \nabla \cdot \mathbf{p} = 0, \tag{3.2}$$

where $\mathbf{p} \equiv a\mathbf{v}$ and **v** is the peculiar velocity, or velocity relative to a rest frame (Peebles, 1980b). The conservation of momentum for an ideal fluid is given by the Euler equation by adding a pressure-gradient force to the equation of motion for a freely-falling mass element (Bertschinger, 1995)

$$\frac{\partial \mathbf{v}}{\partial t} = -\frac{\nabla P}{\rho} - \nabla \phi \tag{3.3}$$

for a generic field or function in proper coordinates, or in co-moving units,

$$\frac{\partial \mathbf{p}}{\partial t} = -a^2 \frac{\nabla P}{\rho} - \frac{\nabla \phi}{a}, \tag{3.4}$$

where ϕ is the scalar potential (Landau & Lifshitz, 1959). Hydrodynamic simulations then close the Euler equations by incorporating the evolution of pressure or some other thermodynamic variable — this is typically applied as the first law of thermodynamics to obey conservation of energy under thermodynamic processes as

$$\frac{\partial u}{\partial t} = -\frac{P}{\rho} \nabla \cdot \mathbf{v} - \frac{\Lambda(u, \rho)}{\rho}, \tag{3.5}$$

where Λ is the proper cooling rate. P, ρ, and the thermal energy per unit mass, u, couple via the equation of state

$$P = (\gamma - 1)\rho u, \tag{3.6}$$

where γ is the adiabatic index and typically set to $\gamma = 5/3$ for an ideal, monatomic gas (Springel & Hernquist, 2002; Somerville & Davé, 2015).

Using the Euler equations coupled with a chosen gravity solver (N-body simulation), hydrodynamical simulations are capable of directly addressing a wide range of dynamical scales and numerically solving the complexity of galaxy formation through the cosmological growth of density fluctuations (Springel, 2010). However, even with the inclusion of baryonic physics, scales ranging between Mpc and astronomical units (AU) cannot be resolved numerically, and all of the relevant physics is happening at scales where semi-analytic approaches are needed to treat the complex processes of star formation and feedback from SNe at the "subgrid" level (Silk et al., 2014).

3.2.2. Hydrodynamical Methods

Hydrodynamical methods are divided into two main classes: Eulerian grids (Laney, 1998; Leveque et al., 1999), which use fixed spatial grids to measure fluid properties with respect to a single reference point, and Lagrangian methods (see, e.g., Gingold & Monaghan, 1977; Lucy, 1977), which measure fluid properties in the reference frame of individual cells.

3.2.2.1. Eulerian Methods

Eulerian methods solve hydrodynamics by discretizing the fluid onto fixed grid cells and computing the transfer of properties across the cell boundaries. Eulerian grid based methods are able to efficiently model fluid mixing and shocks (Agertz et al., 2007), and they are able to resolve important dynamical instabilities such as Kelvin–Helmholtz or Rayleigh–Taylor (Agertz et al., 2007; Price, 2008). Eulerian grid based methods have improved with the adaptive mesh refinement (AMR) scheme (RAMSES; Teyssier, 2002), in which cells satisfy some local criteria (typically based on mass) and are split into sub-cells to improve the resolution in those regions, and as a result, adopt some of the Lagrangian advantages of being naturally adaptive in space and time to achieve higher resolution (Silk et al., 2014; Frenk et al., 1999).

3.2.2.2. Lagrangian Methods

In cosmological simulations, Lagrangian motions of gas particles such as "smoothed particle hydrodynamics" (SPH; Gingold & Monaghan, 1977; Lucy, 1977; Monaghan, 1992) track the motion of gas by calculating gas properties on each particle and averaging over the nearest particles. Individual particles carry information about the fluid that is obtained with a kernel-weighted sum over the nearest neighboring particles

$$X_i = \sum_j m_j (X_j/\rho_j) W(|r_i - r_j|, h_i, h_j), \tag{3.7}$$

where X_i is the quantity to be estimated, m is the particle mass, ρ is the particle density, and W is the smoothing kernel which serves as a spherical function of distance between particles in units of smoothing length (h) (Somerville & Davé, 2015). By evaluating the Euler equations with a smoothing kernel, solutions are simple to implement in three dimensions and scalable to the spatial requirements of simulations. Particle-based methods such as SPH directly track the movement of mass, allowing models to form galaxies and track physical processes such as ejected material and kinetic winds that are often implemented as a subgrid treatment of galactic outflows (Springel & Hernquist, 2003; Springel, 2010).

While Lagrangian methods are more adaptive and offer a dynamic range of model advantages over Eulerian methods in terms of simulation resolution, comparisons of both methods show strengths and weaknesses that depend on the the time-step or integration scheme, initial conditions, and the relative time or mass scale that is being chosen for a particular simulation. Although there is relative agreement on the properties of DM, hydrodynamical properties such as baryon fraction and X-ray luminosity (Frenk et al., 1999; Tasker et al., 2008) are noticeably different between methods, and particle-based methods are limited in mass resolution as different scales are resolved with varying numbers of particles (Dolag et al., 2008). Therefore, resolution becomes significant when addressing key components and properties for a cosmological object or region of interest.

3.3. Simulation Resolution

Relative to DM-only simulations at the same resolution, hydrodynamical simulations require significantly more resources and computation time. As a result, these simulations may be limited to lower resolutions that can introduce uncertainties that make it difficult to isolate and understand key physical processes such as star formation and feedback. As mentioned in Section 3.1, simulation resolution is finite and therefore chosen based on the level of detail that is required. Hydrodynamical simulations are therefore generally divided into two main categories to address a particular region of interest — "Big-Box" and "Zoom-in" simulations.

Big-Box simulations (e.g. Illustris, IllustrisTNG, EAGLE; Nelson et al., 2015; Springel et al., 2018; Schaye et al., 2015) scale above the kpc scale at approximately 100 Mpc and are able to provide large statistical samples by modeling galaxy populations, galaxy clusters, and the large-scale structure of the Universe (Dolag et al., 2008). Due to the large volume of these simulations, they require extensive computational cost and time at a lower resolution. Big-Box simulations typically have particle masses on the order of 10^6 $M_\odot$ or greater, and they have a spatial resolution of approximately 1 kpc (Schaye et al., 2015). These simulations also rely on phenomenological subgrid models, where the anticipated behaviors of physical processes are predicted rather than resolved due to resolution limitations.

Zoom-in simulations (see, e.g., RomulusC, FIRE, DCJL, MARVEL; Tremmel et al., 2017a;

Garrison-Kimmel et al., 2019; Applebaum et al., 2021; Munshi et al., 2021) do not model large-scale structures, but are instead used to model one to a few halos or otherwise isolated regions at a time. Zoom-in simulations achieve much higher resolutions with particle masses on the order of 10^4 $M_\odot$ or greater, and they have a spatial resolution on the order of parsecs (Dolag et al., 2008; Tremmel et al., 2017b). In a cosmological setting, the current state of simulations necessarily require subgrid components to model and resolve star formation and stellar feedback. However, at these scales, key subgrid models begin to resolve at sufficiently high resolution as hydrodynamics allows feedback methods to converge (Springel & Hernquist, 2003). This is particularly important for understanding the details of stellar feedback in dwarf galaxies, as the subgrid physics can significantly impact physical processes and alter the DM response.

3.4. Conclusion

In conclusion, simulations are essential for addressing tensions between theoretical predictions and observational data, particularly when it comes to understanding the complex interplay of baryonic and DM processes. This chapter explored the importance of various simulation approaches, and highlighted their respective strengths and limitations. Chapter 4 will expand on the physical processes used in simulations by introducing star formation recipes and specific feedback mechanisms that are crucial in shaping the evolution of dwarf galaxies and thereby influence their SFHs and DM distributions.

Chapter 4

MARVEL-ous Dwarfs

Portions of this chapter are reproduced from the work of Azartash-Namin et al. (2024), published in *The Astrophysical Journal, 970:40 (14pp)* in collaboration with co-first author Anna Engelhardt and co-authors Ferah Munshi, B. W. Keller, Alyson M. Brooks, Jordan Van Nest, Charlotte R. Christensen, Tom Quinn, and James Wadsley.

4.1. Introduction

As discussed in Section 3.3, subgrid components of cosmological hydrodynamic simulations are necessary to compare predictions of structure evolution processes and observational data. In low-mass systems where subgrid scales begin to resolve, the prescriptions for modeling star formation and stellar feedback becomes crucial to understand the impacts from the interplay of baryons and DM on smaller scales. To understand the effects of baryonic subgrid physics and feedback on DM properties in dwarf galaxy simulations, this work uses a subsample of dwarf galaxies from the "MARVEL-ous Dwarfs" (MARVEL) zoom-in simulations — in particular, one of the four volumes called Storm is used to compare two distinct SN feedback models. The MARVEL simulations generate a large sample of isolated dwarf galaxies at a high resolution (60 pc force resolution), with gas, initial star, and dark matter masses of 1410 $M_\odot$, 420 $M_\odot$, and 6650 $M_\odot$ respectively, which allow for resolving galaxy masses as low as M_{star} ∼6000 $M_\odot$ (Munshi et al., 2021).

The simulations were run from $z = 149$ to $z = 0$ within a WMAP3 cosmology (Spergel et al., 2007) and implement the N-Body + SPH code ChaNGa (Menon et al., 2015) as well as the charm++ runtime system (Kale & Krishnan, 1993) (see A.1,A.2) to scale up to thousands of cores via a tree-based gravity solver.

4.2. Star Formation Properties

Star formation is the driving force behind galactic evolution and spans a wide range of scales from galaxy cluster cores to the entire interstellar medium (ISM). As such, empirical laws to define star formation rates have been a subject of investigation for many decades. The Storm simulations, as with all the MARVEL simulations, reproduce the Schmidt Law (Schmidt, 1959) which derives a star formation rate (SFR) over the history of the MW as

$$f(t) \sum_{M_v} \Psi(M_v) = C[M_G(t)]^n, \tag{4.1}$$

where $f(t)$ is the function for SFR, $\sum_{M_v}$ is a summation over all stellar types, $\Psi(M_v)$ is a constant initial luminosity function for stars as a function of visual magnitude, and M_G is the gas mass as a function of time. This equation illustrates that the SFR scales with gas density, and subsequently, several scaling relations to connect the average surface density of gas and the average surface density of star formation have emerged. The standard empirical relation used in the MARVEL simulations is the Kennicutt-Schmidt Law (K-S; Schmidt, 1959; Kennicutt, 1998) which relates the surface density of star formation to the surface density of atomic hydrogen (HI), molecular hydrogen (H_2), or total gas

$$\sum_{SFR} \propto (\sum_{gas})^n, \tag{4.2}$$

and is routinely used for computational star formation as a result of observational evidence supporting higher star formation efficiency in gas surface densities where molecular hydrogen dominates the gas profile (Christensen et al., 2012). As such, this work incorporates probabilistic star formation that depends on the local abundance of H_2. This is achieved by modifying the probability of a star forming to include a local fraction of H_2 and thereby constrain star formation to regions with ample molecular hydrogen. Following the K-S relation in which the probability of star formation depends on the local density, the probability, p, of a gas particle forming a star is given by

$$p = \frac{m_{gas}}{m_{star}}(1 - e^{-c^* \Delta t / t_{form}}), \tag{4.3}$$

where m_{gas} is the mass of the gas particle, m_{star} is the initial mass of a potential star particle, c^* is the star forming efficiency factor, and t_{form} is the local dynamical time (Stinson et al., 2006). To incorporate the local H_2 abundance and increase the probability of star formation in highly molecular regions, the star formation efficiency is modified to

$$c^* = c_0^* X_{H_2} = 0.1 f_{H_2} = 0.1 \frac{x_{H_2}}{x_{H_2} + x_{HI}}, \tag{4.4}$$

where $x_{H_2}$and x_{HI} are the mass fractions of molecular hydrogen and atomic hydrogen respectively.

Star particles represent stellar populations with a Kroupa (2001) Initial Mass Function (IMF) and initial mass that is 30% that of the original gas particle. To form a star, gas particles are constrained to have temperatures less than 10^3 K and densities $\rho > 0.1$ amu cm^{-3} as they must be sufficiently dense ($\rho \geq \rho_{min}$) and cool ($T \leq T_{max}$) (Christensen et al., 2012). The MARVEL simulations also include dust and self-shielding of H_2 from radiation, as well as dust shielding of HI, to allow molecular gas to form in high-density regions. Additionally, gas cooling of H_2 is integral to the production of cold ISM where efficient star formation takes place (Christensen et al., 2012). Super massive black hole (SMBH) formation, growth, mergers, feedback, and dynamics are also based on local gas conditions (Bellovary et al., 2011; Tremmel et al., 2015, 2017b; Bellovary et al., 2019).

The simulations implement metal cooling and diffusion (Shen et al., 2010) with a time-dependent uniform UV background (Haardt & Madau, 2012). The UV background decreases the metal cooling rate for temperatures above 10^4 K, but below this threshold cooling rates are increased due to a larger number of free electrons. Shen et al. (2010) found that galactic winds most efficiently enrich the intergalactic medium (IGM) for intermediate-mass galaxies between 10^{10} and 10^{11} $M_{\odot}$, and lower mass galaxies remain metal-poor because gas is prevented from efficiently accreting. The process of metal diffusion decreases the metal content in the IGM by mixing winds before they escape, increasing the quantity of low-metallicity gas contained within these winds (Shen et al., 2010).

With this star formation prescription, the MARVEL dwarf galaxy simulations are able to produce cored DM density profiles. In the following sections, the selected galaxies from the MARVEL Storm blastwave and superbubble feedback runs have a minimum of 14 star particles and a minimum extended SFH of 100 Myr.

4.3. Halo Properties

DM halos in the MARVEL simulations are identified courtesy of Anna Engelhardt in the work by Azartash-Namin et al. (2024) with Amiga's Halo Finder (AHF; Gill et al., 2004; Knollmann & Knebe, 2009). Satellite halos are excluded from this work to limit the impact of external mechanisms such as tidal stirring on star formation and gas removal. The virial radius, R_{vir}, is defined as the radius at which the average halo density is 200 times the critical density of the Universe at a given redshift, 200 $\rho_{crit}(z)$. Halo properties are calculated within the virial radius using the AHF catalog and particles within the virial radius are considered bound to the halo unless the particle velocity exceeds the escape velocity.

The PYNBODY analysis code (Pontzen et al., 2013) was used to match Halos between the superbubble and blastwave runs of the simulations by determining the percentage of shared DM particles. Halos are matched if more than 75 percent of the DM particles in a given superbubble halo share the same particle-ID as the DM particles in the corresponding halo from the blastwave run.

4.4. Feedback Methods

Small-scale structures such as dwarfs are unique in that they are extremely sensitive to feedback processes during their evolution. Feedback from SNe and stellar winds is capable of heating and redistributing gas within a galaxy to alter the star formation rate and gravitationally influence the distribution of DM. This ultimately determines the central DM distribution of galaxies and supports the cored density profiles observed in dwarf galaxies.

For this work, the Storm volume is run with two distinct SNe feedback models. The first is a blastwave SN feedback model (Stinson et al., 2006) that mimics the transfer of the kinetic energy of SN shock waves to thermal energy in the ISM. The second model is a superbubble feedback model (Keller et al., 2014) that introduces superbubbles — large, hot, low-density cavities in the ISM or the intergalactic medium (IGM) that form from the combined energy of stellar winds and SN explosions in clusters of massive stars.

4.4.1. SNe Feedback

SN feedback is crucial for regulating star formation, driving galactic outflows, and influencing the structure and evolution of galaxies. In simulations this feedback is necessary to prevent the overproduction of stars and appropriately distribute gas and metals. SN explosions from massive stars inject significant amounts of momentum and energy on the order of 10^{51} ergs into the surrounding gas and the ISM. This expands the surrounding gas with extremely high temperatures and produces shock waves that inject energy into the local ISM. The energy deposited into the local ISM can either be thermal, creating hot "superbubbles" or kinetic "blastwaves" that transfer momentum to the surrounding gas and produce large-scale galactic winds and outflows.

By heating the gas, SN feedback prevents rapid cooling that would produce excessive star formation. In simulations, this "over-cooling problem" where gas cools and condenses too efficiently, produces unrealistic star formation rates that are a key issue in matching stellar population models to observation. Heated gas also slows the rate of star formation as a result of having lower density and higher pressure, making it harder for the gas to gravitationally collapse into the molecular clouds where stars form. The outflows and galactic winds produced by SN feedback expel gas from a galaxy into the surrounding environments, regulating the available gas for star formation and enriching the CGM and ISM with metals. Metals increase the cooling efficiency of gas due to radiation energy, further impacting the formation of stars. Galactic winds are especially important in smaller systems where the gravitational potential is weaker and gas can escape more easily.

As star formation occurs in dense gas regions, if SN energy is distributed to nearby gas particles as pure thermal energy, gas is radiated away too quickly and provides no effective feedback. As a result, simulations that directly inject SN energy into the surrounding gas do not produce realistic star formation (Katz, 1992). To address this, sub-resolution schemes for the distribution of SN energy as a feedback on star formation were introduced — as SNe are the direct result of star formation, they can be used as the feedback that limits star formation to produce observed star formation rates.

4.4.1.1. Blastwave

Blastwaves from SNe are used to model the effects of stellar feedback on gas dynamics, regulate star formation, and act as the driving force behind galactic winds and outflows as described in Section 4.4.1. Blastwaves cycle through different evolution phases, beginning with free expansion in which SN ejecta expand into the surrounding medium. When a SN event occurs, the outer layers of a star are ejected at high velocities into the surrounding gas. The gas then heats and compresses, forming material into thin and dense shells.

Blastwaves then enter the Sedov-Taylor phase, where material is continuously swept up from the surrounding medium. This expansion process occurs adiabatically, in which the expanding blastwave experiences a decrease in temperature and pressure without significant radiative losses, conserving energy in the SN remnant because it can't effectively radiate. As the accumulation of material increases, the blastwave begins to lose acceleration and the radius of the shock front scales with time. The Sedov-Taylor phase lasts tens of thousand of years, but the hot, low-density shell survives long after. During a radiative cooling phase, gas behind the blastwave begins to radiate energy away through emission processes and slows the expansion of the SN remnant. The blastwave reaches maximum extent during the snowplow phase, after the gas is cool enough for effective radiation and expansion occurs at a much slower rate. Gas continues to cool adiabatically after the SN remnant reaches full expansion, and the cooled and compressed shell of material in the blastwave becomes denser with gas from the surrounding medium. The blastwave eventually dissipates into the surrounding ISM or IGM.

In this work, the blastwave model (McKee & Ostriker, 1977; Stinson et al., 2006) incorporates individual SNe blastwaves as stellar feedback to appropriately regulate star formation for galactic SPH simulations. The blastwave model directly injects nearby gas particles with mass, metals, and a fixed fraction of the total energy from each supernovae in the form of thermal energy at 1.5×10^{51} ergs per SNe event. The number of SNe is calculated from the IMF of each star particle and it is assumed that only stars with masses ranging from 8 to 40 $M_\odot$ undergo type II SNe.

Cooling in particles within a blast radius is temporarily turned off through the snowplow phase to prevent the numerical over-cooling of energy deposited in the local ISM (Stinson et al., 2006) by limiting the loss of thermal energy from SN through radiative cooling in the surrounding gas particles (see also Brook et al., 2004). The number of particles with cooling disabled depends on an analytic treatment of blastwaves (McKee & Ostriker, 1977). Particles outside of the blast radius have enhanced mass and metallicity, but experience immediate radiative thermal cooling.

In practice, invoking blastwaves has successfully produced cored density profiles in dwarf galaxy simulations (Shen et al., 2014), as they drive gas out of the central regions of galaxies and alter the gravitational potential to redistribute DM into cores. Simulations implementing blastwave feedback are also able to reproduce observed star formation rates and stellar masses (Stinson et al., 2006; Guedes et al., 2011; Munshi et al., 2013, 2021), though Keller et al. (2015) find that blastwave feedback alone does not sufficiently to regulate star formation in L^* galaxies with masses comparable to the MW. Additionally, blastwave models are resolution dependent as simulations cannot resolve individual SNe and do not account for physical processes that occur in nature such as clustered star formation (Nath & Shchekinov, 2013; Sharma et al., 2014).

4.4.1.2. Superbubble

Superbubbles form when massive stars clusters (typically OB stars) undergo successive SN explosions or emit intense stellar winds. Like SN blastwaves, these events inject energy into the surrounding gas and compress the surrounding material. When these events occur in a cluster, the individual SN remnants merge, thermalize, and form superbubbles. Stellar winds from OB stars in the cluster can also combine with SN events to further drive the expansion of superbubbles. In cosmological simulations, superbubbles are an essential component for modeling feedback mechanisms and understanding how SNe impact galaxy formation, the ISM, and the surrounding IGM.

SN remnants are approximately 10 pc in diameter and significantly impact their surroundings, but emerging superbubbles can span hundreds of parsecs and directly influence regions in the ISM or CGM. The gas inside of superbubbles has low density and reaches temperatures on the order of 10^6 K or greater. Consequently, the hot gas expands and drives shocks into the surrounding gas that is much cooler to form an expanding shell of compressed material, resulting in sharp temperature gradients. This expansion is a highly energetic process that can trigger secondary star formation in the compressed gas of the surrounding shell or otherwise cause significant mass loss from galaxies from the removal of gas. Superbubbles lifetimes can last millions of years depending on the availability of new energy sources such as additional SNe. These structures continue to expand until energy dissipates, allowing the superbubble to slow down, cool, and eventually mix into the ISM.

The superbubble feedback model introduced in Keller et al. (2014) and used in this work introduces thermal conduction, subgrid evaporation, and subgrid multiphase treatment to model the early stages of superbubbles in the case of low mass resolution within the simulation. Thermal conduction produces the expected interior densities of superbubbles by accounting for temperature gradients to produce correct interior densities, evaporation processes, and implementing a separate hot and cold phase treatment of gas. Thermal conduction achieves this by maintaining uniform temperatures in hot bubbles while a two-phase treatment of gas particles prevents over-cooling and reduces the model's reliance on subgrid machinery. Evaporation from thermal conduction accurately regulates the quantity of hot gas without the addition of an un-physical cooling shutoff and the model is insensitive to resolution. This work follows the treatment of energy per SNe event outlined by Keller et al. (2015) and reproduced by Mina et al. (2021) to follow the heating time associated with SNII from OB stars with 10^{51} ergs per SNe event. As a result, the superbubble model initially injects less thermal energy into the surrounding gas particles than the blastwave model.

4.5. Discussion

Keller et al. (2014, 2015); Keller (2022) found that simulations run with a blastwave feedback model produce halos with over-massive stellar populations while the superbubble feedback model produces more massive outflows that efficiently expel low angular momentum gas from the centers of MW-mass galaxies. Effective expulsion of low angular momentum gas particles at high red-shift limits star formation at the centers of galaxies, subsequently avoiding the creation of overly-massive stellar bulges (Governato et al., 2010b; Brook et al., 2011; Christensen et al., 2014). As a result, superbubble galaxies are more disk dominated than blastwave galaxies (Keller et al., 2015) and have less centrally dense stellar populations (Keller et al., 2015; Keller, 2022).

Keller et al. (2014, 2015); Keller (2022) also found that the superbubble feedback model shows stronger star formation regulation by reducing star formation rates by a factor of two relative to the blastwave model and is more effective at driving mass-loaded outflows by roughly an order of magnitude. This feedback model is potentially a solution for modeling galaxies within the ΛCDM framework without the use of unphysical cooling shut-offs.

Mina et al. (2021) found within a small sample of dwarf galaxy masses that the superbubble model implements the physics behind SNe feedback processes more accurately than the delayed cooling shutoff for blastwave. This subsequently reproduces reasonably realistic dwarf galaxies with comparable stellar and gas properties that are observed within the Local Volume. As discussed in Section 4.2, this work adopts a star formation prescription based on the local abundance of H_2, which is more physically motivated than the one used by Mina et al. (2021) and likely allows the ISM to reach higher densities and cooler temperatures.

4.6. Conclusion

In summary, the implementation of feedback mechanisms plays a crucial role in shaping the structure and evolution of dwarf galaxies. This chapter detailed how different feedback models impact star formation and DM profiles, providing essential context to the importance of finding agreement between models and observations and understanding the relationship between feedback processes and bursty SFHs. In Chapter 5, this work expands upon this treatment of stellar feedback implementation by directly calculating burstiness values and DM cores for two distinct SN feedback methods. A full sample of dwarf galaxy masses are sampled using the MARVEL zoom-in simulations that contain dozens of dwarfs ranging from LMC-mass down to the ultra-faint dwarf mass regime. For the comparison of bursty feedback and DM core formation, the Storm sample of dwarf galaxies was analyzed with two separate simulation runs: one that implements blastwave feedback and a second that implements superbubble feedback. The sample in this work consists of a total of 19 dwarfs in the superbubble run and 21 in the blastwave run.

CHAPTER 5

Bursty Star Formation

This chapter is reproduced from the work of Azartash-Namin et al. (2024), published in *The Astrophysical Journal, 970:40 (14pp)* in collaboration with co-first author Anna Engelhardt and co-authors Ferah Munshi, B. W. Keller, Alyson M. Brooks, Jordan Van Nest, Charlotte R. Christensen, Tom Quinn, and James Wadsley.

5.1. Introduction

Dwarf galaxies often exhibit bursts of star formation as a result of stellar feedback, in which stars form in episodic bursts rather than the steady formation seen in large, self-regulating galaxies. Bursty star formation, or "burstiness", can have a significant impact on the distribution of DM in dwarf galaxy halos and as a result, has the potential to resolve key tensions between ΛCDM predictions and observation regarding the DM cored density profiles in low-mass galaxies.

5.1.1. Dark Matter Cores

Under certain conditions, fluctuations in the gravitational potential can result in a cuspy DM density inner profile that flattens to a more cored profile. Pontzen & Governato (2012) find that rapidly expanding gas as a result of bursty star formation allows models to reveal central potential fluctuations capable of generating DM cores. Sales et al. (2022) discuss how DM core formations in cosmological simulations are commonly revealed when resolving star formation with high gas density thresholds, that also result in bursty star formation.

Dutton et al. (2019) show that star formation becomes burstier and more clumped for higher star formation density thresholds. However, the burstiness of star formation alone is not sufficient for core formation. Instead, core formation occurs when high gas densities are resolved and star formation is restricted to occur at high densities. Jahn et al. (2023) find cores are capable of forming when star formation density thresholds are set low, but affirm that cores only form when a multiphase ISM that resolves sufficiently high density contrast is resolved.

The blastwave and superbubble simulations in this work adopt star formation prescriptions that have been shown to create DM cores (Governato et al., 2010b, 2012; Shen et al., 2014; Mina et al., 2021). The range of temperatures for gas particles in the blastwave run of the simulation is $10 < T < 2.3 \times 10^6$ [K] and $10 < T < 6.8 \times 10^4$ [K] for superbubble. Gas particle densities range from 10^{-14} amu cm^{-3} to 435 amu cm^{-3} at redshift $z = 0$. However, the ability to form a DM core also depends on the stellar mass of the galaxy, as the stellar mass sets how much SN feedback is available to induce fluctuations in the gravitational potential. A number of studies have found that inner DM density slopes depend strongly on the mass ratio of stellar mass to total halo mass, M_*/M_{halo}. In general, most simulations find a characteristic mass-ratio for peak core formation at $M_*/M_{halo} \simeq 5 \times 10^{-3}$ (Di Cintio et al., 2014; Chan et al., 2015; Tollet et al., 2016; Lazar et al., 2020), where values above and below this fall back into the the 'cuspy' density profiles that are prevalent with DM-only simulations.

To address the slowly rising rotation curves of dwarf galaxies that are best characterized by cored profiles, Lazar et al. (2020) introduced a three parameter core-Einasto profile, as discussed in Section 1.2.3, that includes a radius-core parameter (r_c) to parameterize the density profile of the entire halo and define where the profile begins to flatten into a constant-density core. This work adopts the core-Einasto profile to analyze the inner DM density core slopes (α) of the Storm halos, where the slope characterizes the rate at which the DM density changes as a function of distance from the center of the halo. Slopes are calculated from the best fit core-Einasto model at 1-2% $R_{\rm vir}$ to capture the gradient of the DM density at small radii. For the halos presented in this work, $\alpha = 0$ for cored (constant density) profiles, followed by shallower core slopes. As core slopes become steeper, or more negative as they approach -1, they become cuspier. To further investigate the nature of core formation, the following sections introduce a burstiness parameter and explore a relationship between burstiness and DM core slopes.

5.1.2. Quantifying Burstiness

Dwarf galaxy simulations that include baryonic physics predict that feedback-induced DM cores result from bursty star formation driving rapid gas outflows and core formation is sustained with multiple starburst cycles (Read & Gilmore, 2005; Pontzen & Governato, 2012). To investigate the Storm halos over the entire cosmic timescale, or the Hubble time, this work implements a burstiness parameter:

$$B = \frac{\sigma/\mu - 1}{\sigma/\mu + 1}$$

where σ is the standard deviation of the supernova rate and μ is the mean supernova rate (see also Applebaum et al., 2020). Thus burstiness ranges from -1 to 1 where a uniform distribution, or the supernova rate = 0, has a burstiness B = -1 and an exponential distribution has a burstiness B = 0. Burstiness will approach 1 as $\sigma/\mu \rightarrow \infty$.

The supernova rate is calculated in 1 Myr increments for the age of the Universe for all halos within the simulations. The rate is calculated for the first 50 Myr of star formation to coincide with the approximate cooling shut-off time for SNe feedback in our simulations. The burstiness of the SN rate is averaged over this windowed timescale of 50 Myr from the first star forming particle to the current age of the Universe. This timescale is selected to be on order of the scale of the feedback timescale, or put another way, the typical age of an O or B star. For halos that have truncated SFHs (in particular, UFDs) we find that B is robust to averaging timescale; for halos with continuous SFHs, we find that B is in fact sensitive to averaging timescale. However, for values of averaging timescale that vary within 10-500 Myr, B changes by only a factor of 2. Timescales the length of one Gyr and longer result in all halos having non-bursty B values.

To determine if there is relation between DM cores and burstiness, core slopes and the average burstiness values of the SN rates for each halo in the simulations were directly compared as functions of the stellar mass fraction, M_*/M_{halo}. Initially, this relation was analyzed for the entire suite of MARVEL dwarf galaxies using the blastwave feedback method. Figure 5.1 shows burstiness and core slopes relative to M_*/M_{halo} for the entire MARVEL suite of simulations (Storm, Elektra, Rogue, and Captain Marvel), revealing a general trend between burstiness values and the DM core slopes of the MARVEL dwarfs.

In contrast with the burstiness calculated over a Hubble time, "active burstiness" was defined within the timescale of active star formation for a given halo. Burstiness calculations were confined to time bins between the formation of the first star particle and the last star formation. The average burstiness during active star formation and α[1-2%]r_{vir} DM density slopes are shown as functions of M_*/M_{halo} in Figure 5.2 for the entire MARVEL suite using blastwave feedback, revealing that UFDs are burstier during active star formation relative to the age of the Universe and form the majority of their stellar populations in a single burst early on.

The Storm simulation was ultimately chosen for the comparison of the two feedback models for both the cosmic timescale and timescale of active star formation due to the diversity of its mass range, and the remaining content of this work only includes the Storm simulation to compare the burstiness and core slopes for the blastwave and superbubble feedback methods. As discussed in Section 5.1.1, inner DM density profiles have been shown to depend on the stellar mass fraction, M_*/M_{halo}. Figure 5.3 shows the DM core slopes for both feedback models relative to burstiness with the corresponding stellar mass to determine the significance of sustained bursty star formation and DM cores. The burstiness and core slopes for each Storm halo during active star formation is directly compared to the burstiness for the cosmological timescale in Figure 5.4.

To provide potential insight into a time frame that is relevant to current observations, instantaneous burstiness was calculated as the burstiness within a selected Δt between the last 100 Myr of the Storm simulations. The last two burstiness measurements of the simulation are are separated by 50 Myr and averaged as a proxy for an instantaneous burstiness measurement at z = 0. This work found no direct correlation between instantaneous burstiness and core slopes for the entire range of halo masses, although it is worth noting that there was a distinct mass cutoff for the ultra-faint mass regime as shown in Figure 5.5. Instantaneous burstiness appears to be reflective of the star

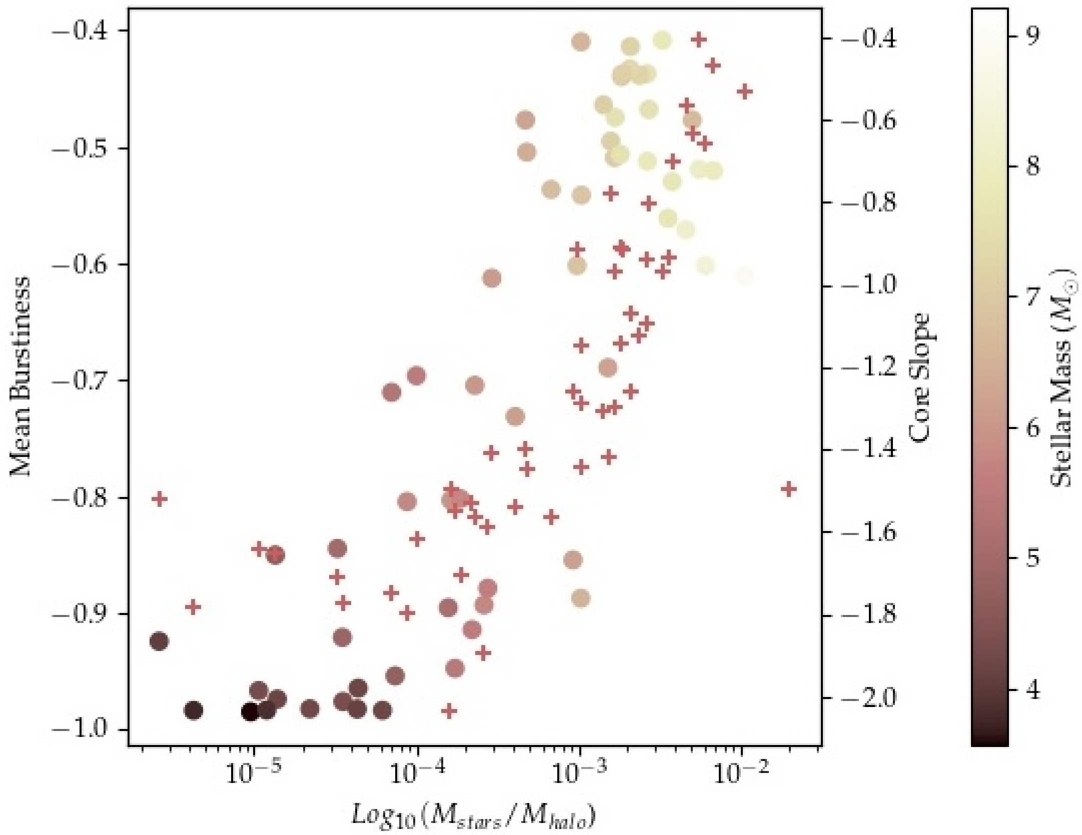

Figure 5.1: α[1-2 %]r_{vir} Core-Einasto core slopes (given by the + symbols) and burstiness values (given by the colored points) as a function of the stellar mass fraction, M_*/M_{halo}, for the entire MARVEL suite of dwarf galaxy simulations: Storm, Elektra, Rogue, and Captain Marvel using the blastwave feedback method. Burstiness values for each halo are colored according to stellar mass, ranging from UFDs shown in dark brown, up to bright dwarfs in pale yellow, with classical dwarfs in between. This plot introduced a novel comparison of the general trend between burstiness and DM core slopes for a full suite of zoom-in, high resolution simulations of the MARVEL dwarf galaxies using blastwave feedback. The Storm simulation was later chosen for comparing feedback models due to having the most diverse mass range and largest DM halos to capture the entire mass scale of dwarf galaxies.

formation history in the few Myr prior to the last time-step, indicating that the ultra-faint dwarf galaxies in the Storm simulation become quenched early on and do not have sustained bursty star formation throughout the chosen timescale.

5.2. Results

Figure 5.6, produced by co-first author of Azartash-Namin et al. (2024), Anna Engelhardt shows the DM density slopes of the Storm simulations for both feedback models in comparison to other simulations that have incorporated baryonic feedback as well as a DM-only simulation.

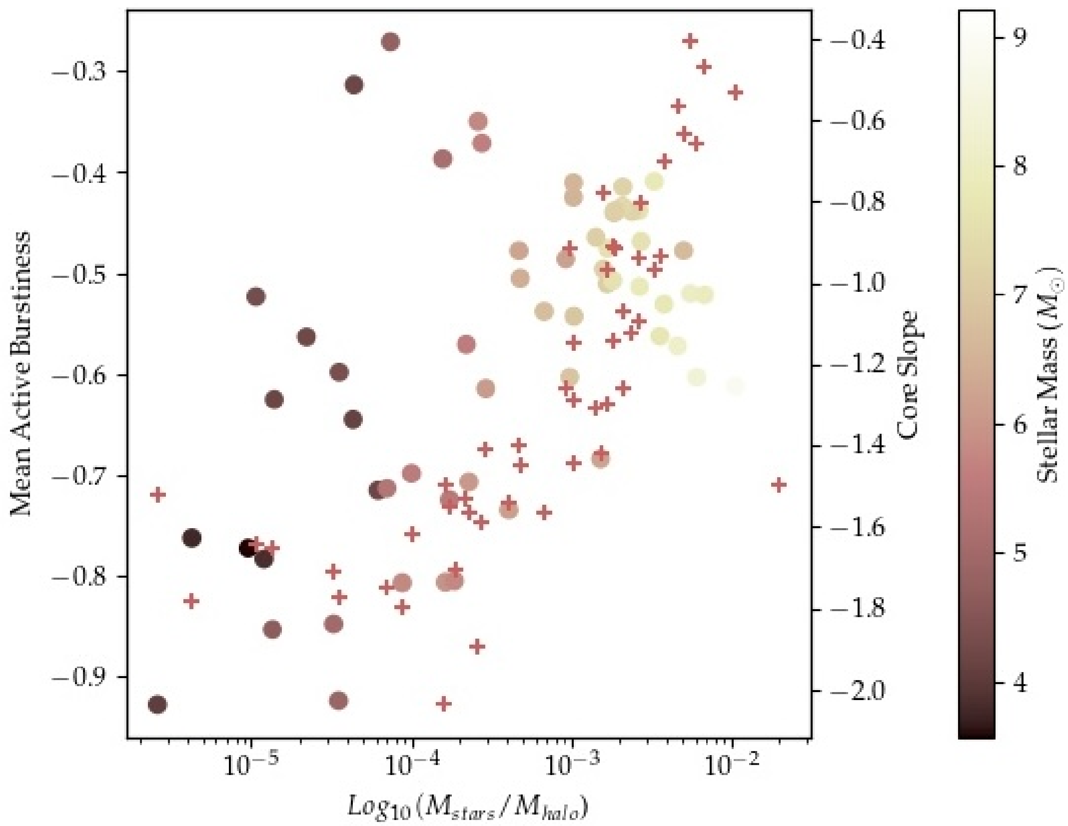

Figure 5.2: α[1-2 %]r_{vir} Core-Einasto core slopes (given by the + symbols) and burstiness values (given by colored points) relative to the stellar mass fraction, M$_*$/M$_{halo}$, during active star formation for the entire MARVEL suite of dwarf galaxy simulations: Storm, Elektra, Rogue, and Captain Marvel using the blastwave feedback method. Burstiness values for each halo are colored according to stellar mass, ranging from UFDs shown in dark brown, up to bright dwarfs in pale yellow, with classical dwarfs in between. This plot introduced a novel comparison of the general trend between burstiness and DM core slopes during the time period of active star formation for MARVEL dwarf galaxies using blastwave feedback. UFDs are significantly burstier during active star formation due to their stellar populations generally forming in one large burst early on.

Engelhardt found that the superbubble (red circles) and blastwave (blue squares) feedback models are indistinguishable from each other, with flatter core-slope values relative to the halos studied in Lazar et al. (2020), represented by the black triangles, and slopes that steepen less quickly with declining M$_*$/M$_{halo}$. The Storm simulations best matched the DM density profile fit from Di Cintio et al. (2014), represented by the gray shaded region, and were found flatter, or closer to $\alpha = 0$, than the profile shape in Tollet et al. (2016) given by the pink band. As discussed in Section 3.1.1, Figure 5.6 also confirms that DM-only simulations, represented by "$\times$" symbols, produce cuspy central cores around $\alpha = -1.5$ in contrast with models incorporating SPH and hydrodynamics codes that produce core slopes approaching $\alpha \sim 0$, indicating that the baryonic subgrid physics used in the

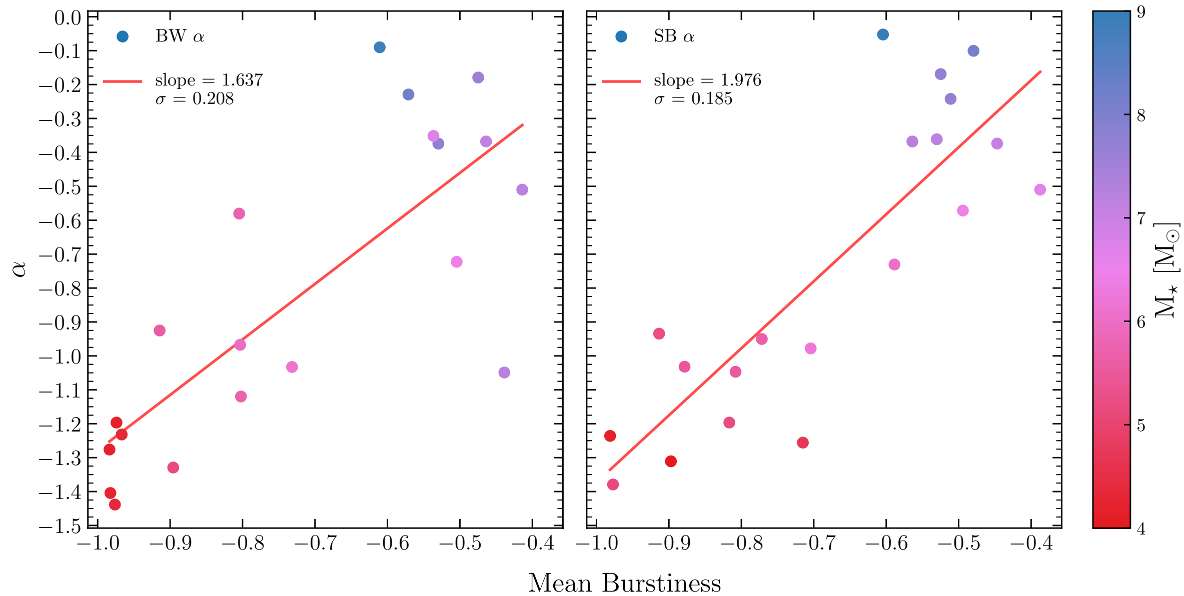

Figure 5.3: α[1-2 %]r_{vir} Core-Einasto fit core slopes of the Storm DM halos (colored points) as a function of burstiness for the Storm simulation dwarf galaxies. Core slopes are colored by $M_\star$ [$M_\odot$] to correspond to bright (blue), classical (pink), and ultra-faint dwarfs (red). The left panel shows core slope values for Storm simulation using the blastwave feedback method and the right panel shows the superbubble feedback method. The standard deviation (σ) was calculated to quantify which feedback model had less scatter, indicating a tighter relation between core slope and average burstiness. The superbubble model reveals slightly less scatter overall at σ = 0.19 but shows more scatter for UFDs, indicating that core slopes depend less on burstiness.

Storm simulations can address tensions with the cusp-core problem by overall being in agreement with other simulations that use baryonic feedback, while also producing DM cores closer to $\alpha \sim 0$ relative to others.

Figure 5.7, produced by co-first author Anna Engelhardt (Azartash-Namin et al., 2024), reveals that the higher-mass dwarf galaxies from the bright dwarf regime steadily form cores over time in contrast with classical and ultra-faint dwarfs that do not experience the sustained star formation required to produce cores. Figure 5.7 also shows that ultra-faints are significantly cuspy throughout their lifetimes whereas classical dwarf galaxies may form temporary cores before reverting back to cuspy profiles, as shown in the middle panel of Figure 5.7, where some halos approach $\alpha \sim 0$ before reverting back to cuspier (more negative) values. Jackson et al. (2024) find that repeated bursts of star formation result in the creation of cores in stages for galaxies where the central mass of gas is comparable to DM. The formation of cores in the Storm simulations is similarly restricted to halos which are more gas rich. It was determined in this work that at least 1% of the total halo mass was composed of gas for Storm halos with core slope values above -0.5 in both feedback

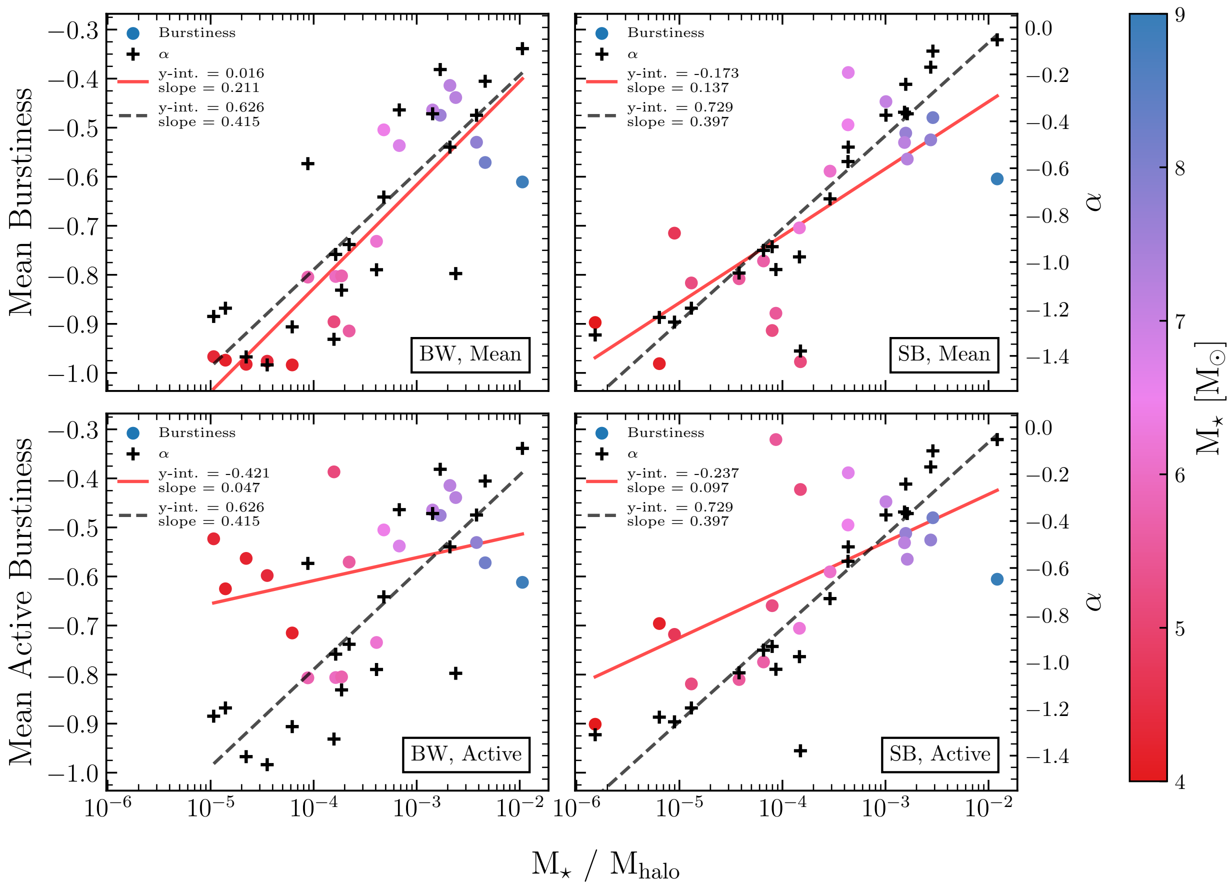

Figure 5.4: Burstiness (colored points) and α[1-2 %]r_{vir} DM core slopes (+ symbols) as a function of halo mass M_*/M_{halo} for the Storm dwarf galaxies. Burstiness values are colored by $M_\star$ [$M_\odot$] where bright dwarfs are represented by blues, classical dwarfs are represented by pinks, and UFDs are represented by reds. Rows separate halos by simulation timescale (top: age of the Universe, bottom: active star formation only) and columns separate halos by feedback model. Burstiness ranges from -1 to 1 where a uniform distribution (supernova rate = 0) has a burstiness B = -1 and an exponential distribution has a burstiness B = 0. The supernova rate was calculated for a non-stochastic IMF in 1 Myr increments for the age of the Universe. Burstiness timing was averaged every 50 Myr beginning at every galaxy's star formation and ending at z = 0. Maximum values of burstiness occur at lower values of M_*/M_{halo} for the superbubble model during the entire cosmic timescale, indicating that core formation may be less motivated by bursty star formation. For the active star formation timescale, the blastwave model shows higher burstiness values for the ultra-faint mass regime, indicating that UFDs are more sensitive to the subgrid physics of blastwave feedback.

runs. Figure 5.7 provides new insight on the mass regime of dwarf galaxies that can sustain cores throughout cosmic time regardless of feedback model, which is shown to fall under the bright dwarf mass regime.

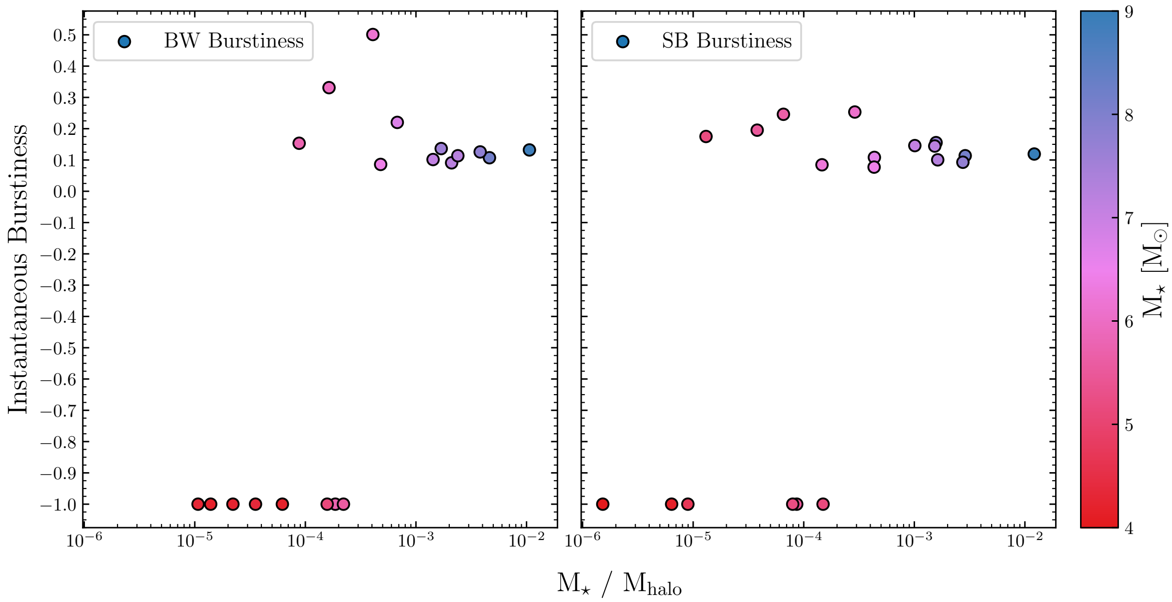

Figure 5.5: Instantaneous burstiness as a function of the stellar mass fraction for the Storm halos. Plots are colored by $M_\star$ [$M_\odot$] and columns separate halos by feedback model. Instantaneous burstiness appears to be reflective of the star formation history in the few Myr prior to the last time-step, indicating that UFDs in the Storm simulation become quenched of star formation early on.

In addition, a relationship between burstiness and α DM cores as a function of halo mass becomes evident in the Storm DM halos. Figure 5.3 illustrates the relationship between core slope and mean burstiness, showing less scatter for the superbubble sample than for the blastwave sample with standard deviation values of 0.19 and 0.21, respectively. The large scatter in both feedback models indicates that core slopes may not strongly depend on burstiness. Although the superbubble model exhibits slightly less scatter overall, the UFD population for this feedback method shows more scatter relative to blastwave, indicating that core formation for UFDs is less dependent on burstiness. Burstiness values (given by colored points) in Figure 5.4 increase with M_*/M_{halo} and directly influence the DM profiles by transforming from cuspier values (more negative) to feedback-induced cores (closer to α=0) , as shown by the core slopes (α) for higher mass dwarfs as colored by $M_\star$ [$M_\odot$].

In Figure 5.4, the DM core slopes (given by + symbols) increase with the stellar mass fraction (M_*/M_{halo}) for both the superbubble and blastwave models. As cores are produced by SN energy driving repeated outflows, the relation between cores and stellar mass may indicate that feedback is under-injected or over-injected into the surrounding gas particles for the blastwave model. The superbubble feedback model shows a roughly linear relation between the stellar mass fraction and core slope, indicating that the subgrid physics produces cored values more efficiently. To further

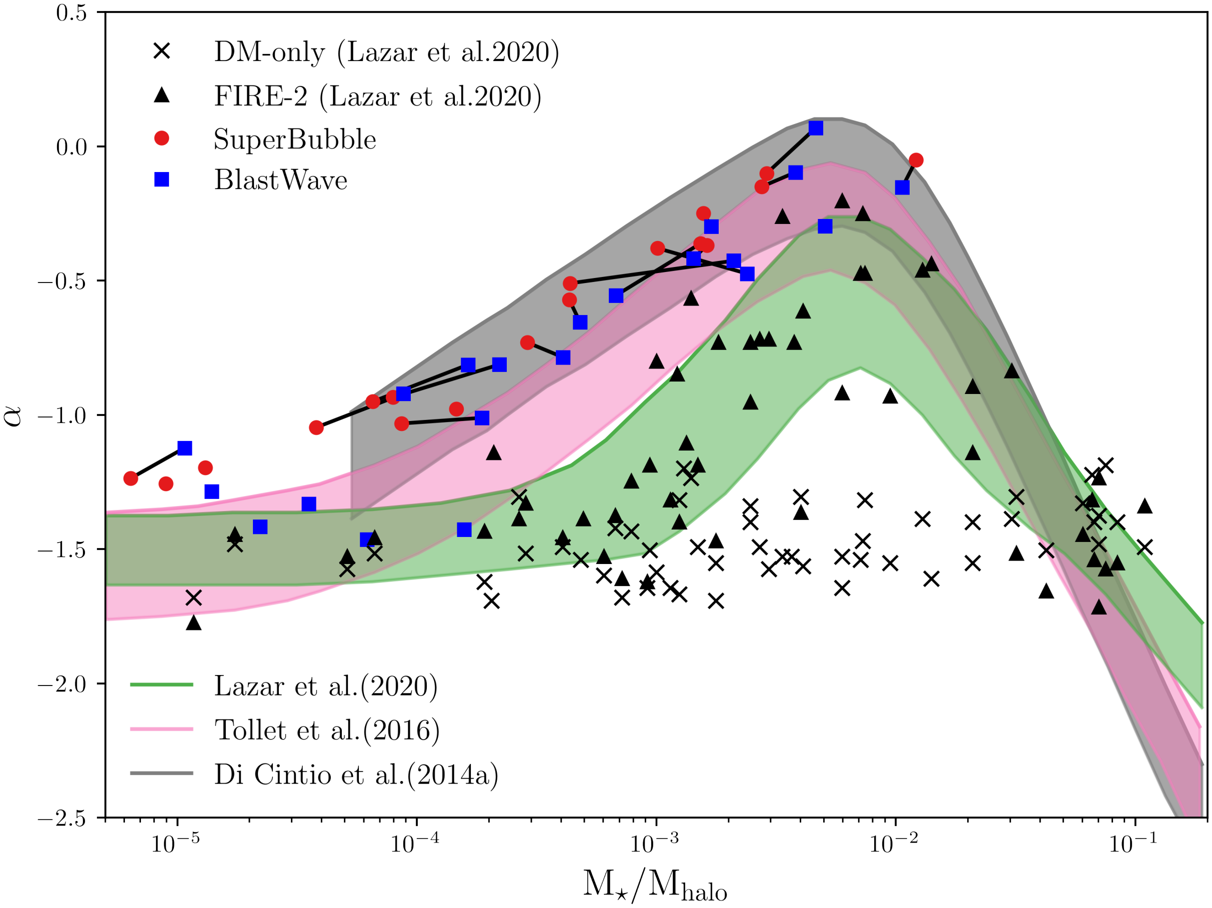

Figure 5.6: DM density profile slopes as a function of M_*/M_{halo} for the Storm simulations, produced by co-first author Anna Engelhardt (Azartash-Namin et al., 2024). Superbubble feedback and blastwave feedback are denoted by red circles and blue squares, respectively, and DM halos are matched with black lines following the prescription outlined in Section 4.3. The Storm profiles are compared with the results from Di Cintio et al. (2014); Lazar et al. (2020); Tollet et al. (2016) in the colored shaded regions representing DM density profile fits based on a mean relation between core slope and M_*/M_{halo}. The FIRE simulation halos are represented by black points, with triangles incorporating baryonic physics and "×" symbols representing halos from DM-only simulations (Lazar et al., 2020). All slopes in this plot are measured at 1-2% R_{vir}, and cuspy density profiles have lower values of $\alpha \leq -1$, while cored profiles have $\alpha \sim 0$. The DM-only simulation shown by "×" symbols produces cuspy profiles, as expected from the NFW profile. All of the simulations incorporating baryonic physics find that DM core creation is maximized for $M_*/M_{halo} \sim 5 \text{ x } 10^{-3}$, where core slopes above and below this value become more negative (cuspy).

illustrate the relation between core slopes and the stellar mass fraction, a linear regression model was used to calculate the y-intercepts, slopes, and the coefficients of determination (R^2) for burstiness values and core slopes with the linear fits given by the red lines (burstiness) and black dashed lines (α) in Figure 5.4. In particular, the R^2 values were used to determine the proportion of the variation

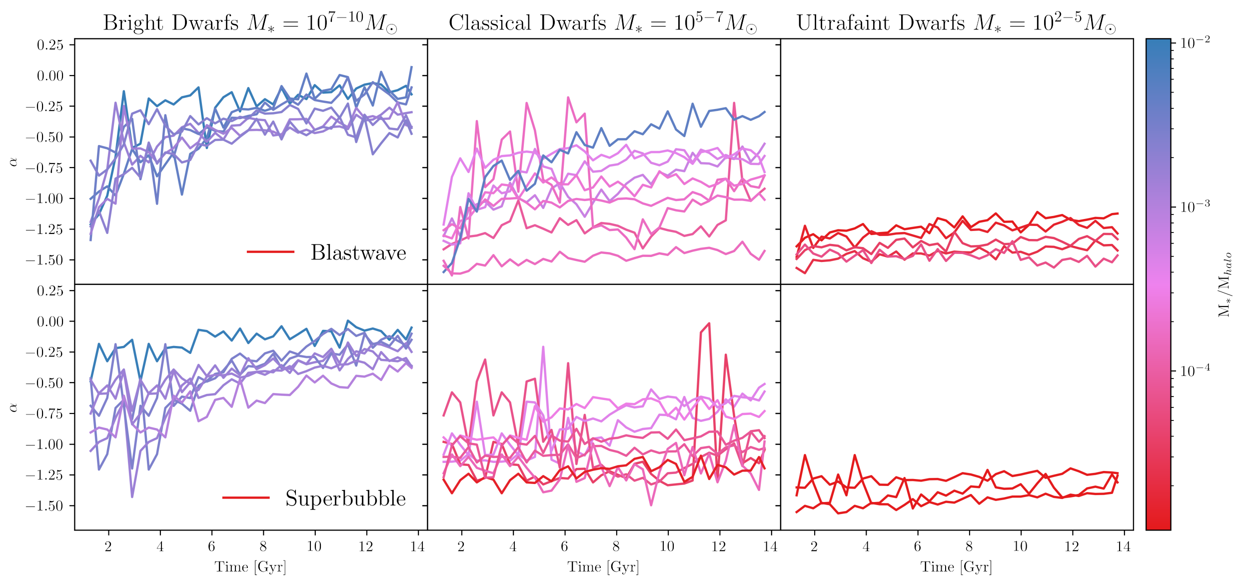

Figure 5.7: Core-Einasto fit slopes (see Section 1.2.3) of the Storm simulations, produced by co-first author Anna Engelhardt in the work by Azartash-Namin et al. (2024). Stellar mass ranges as bright, classical, and ultra-faint as described in Section 2.2 in accordance with Lazar et al. (2020). The leftmost column contains the most massive dwarfs ($10^7 M_*[M_\odot] - 10^{10} M_*[M_\odot]$), the middle column contains dwarfs in the stellar mass range $10^5 M_*[M_\odot] - 10^7 M_*[M_\odot]$ and the least massive dwarfs ($10^2 M_*[M_\odot] - 10^5 M_*[M_\odot]$) are shown in the rightmost column. The top row corresponds to halos run using blastwave feedback while the bottom row shows halos run using superbubble feedback. Plots are colored by M_*/M_{halo}, revealing that higher stellar mass fractions (blue and purple) sustain cores throughout time, whereas the majority of classical (pink) and ultra-faint (red) dwarfs either cycle between cores and cusps or remain cuspy.

in burstiness and core slope values as predicted from the stellar mass fraction in order to formally quantify how well the stellar mass fraction could predict a burstiness or core slope value. R^2 ranges from 0 to 1, with values above approximately 0.7 indicating a relatively good fit and a value of 1 meaning that the statistical model can produce a statistically significant fit and predict the outcome in the linear regression setting. In the case of Figure 5.4, the closer the R^2 is to 1, the better the stellar mass fraction is able to predict a burstiness or core slope value.

Figure 5.4 reveals that the average burstiness for both feedback models show a correlation with α core slopes as a function of the stellar mass fraction. R^2 is equal to 0.75 for burstiness in the blastwave feedback model, which indicates that burstiness depends strongly on the stellar mass fraction. R^2 is equal to 0.67 for core slopes in the blastwave feedback model, indicating that the burstiness values are more motivated by the stellar mass fraction for this feedback model. For the superbubble model, R^2 is equal to 0.55 for burstiness values, which indicates that burstiness has a lesser dependence on stellar mass. With R^2 equal to 0.85 for superbubble feedback, this suggests that core slopes have a stronger correlation to M_*/M_{halo} and are less motivated by bursty star formation.

The average burstiness during active star formation shown in Figure 5.4 shows a different outcome with the superbubble model resulting in a higher R^2 value for burstiness at 0.40 and 0.10 for blastwave feedback. The superbubble model shows less scatter between the core slopes and the stellar mass fraction during active star formation, further supporting that superbubble feedback may have a stronger dependence on $\mathrm{M}_*/\mathrm{M}_{halo}$. In addition, UFDs are significantly burstier during active star formation, with no obvious relation to the core slope values and support the fact that UFDs experience a burst of star formation early on before quenching. This is apparent when comparing UFDs in the top and bottom row of Figure 5.4, as UFDs are not bursty throughout the cosmic timescale.

The ultra-faint mass regime revealed lower burstiness values for the Hubble time, indicating that both models predict the lowest mass dwarfs form the majority of their stellar populations in one large burst at high redshift, and are quenched in more recent years. Blastwave burstiness reaches a maximum value at $\mathrm{M}_*/\mathrm{M}_{halo} \simeq 2 \times 10^{-3}$, just below the threshold of core formation. In the superbubble model, mean burstiness reaches a maximum value at a lower value of $\mathrm{M}_*/\mathrm{M}_{halo} \simeq 4 \times 10^{-4}$. These results indicate that core formation may be better predicted by the stellar mass fraction than burstiness for superbubble feedback. It is worth noting that the tight relationship between stellar and halo mass with core slope indicates that core formation may have a greater dependence on $\mathrm{M}_*/\mathrm{M}_{halo}$. The superbubble model gives a less scattered relation overall between core slopes and $\mathrm{M}_*/\mathrm{M}_{halo}$ relative to the blastwave model, again indicating that core formation with superbubble feedback may have a stronger dependence on the stellar mass fraction.

This work reveals that core formation is robust to feedback model choice, with both superbubble and blastwave simulations producing comparable cores. Additionally, values of $\mathrm{M}_*/\mathrm{M}_{halo}$ between 2×10^{-3} and 2×10^{-2} for both blastwave and superbubble feedback produce cored galaxies with peak core formation occurring at $\mathrm{M}_*/\mathrm{M}_{halo} \sim 5 \times 10^{-3}$ in agreement with the fits produced by (Di Cintio et al., 2014; Tollet et al., 2016; Lazar et al., 2020). In contrast, Jackson et al. (2024) do not find a relationship between increasing core formation with $\mathrm{M}_*/\mathrm{M}_{halo}$ in the NewHorizon (NH) galaxies. They show that NH galaxies with extended, bursty SFHs exhibit cored profiles above a specific halo mass threshold ($\sim 10^{10.2}\ \mathrm{M}_\odot$) but also find that galaxies with cuspy central densities exist across a wide range of $\mathrm{M}_*/\mathrm{M}_{halo}$ values. The Storm simulations produce peak core values at lower $\mathrm{M}_*/\mathrm{M}_{halo}$ ($\sim 5 \times 10^{-3}$) than the mass range and median $\mathrm{M}_*/\mathrm{M}_{halo}$ value presented in Jackson et al. (2024).

Additionally, Jackson et al. (2024) find that sustained star formation at the center of galaxies can increase the central potential and cause DM to cool adiabatically, re-forming a cusp. Jackson et al. (2024) indicate that the relation between α and $\mathrm{M}_*/\mathrm{M}_{halo}$ may be obscured because NH galaxies over-produce stars, however, because core production occurs at similar halo and stellar masses relative to other simulations they argue that core-formation is not solely dependent on stellar mass normalized by halo mass. It is worth noting that the core slope values of the Storm simulations follow a trend of increasing core slope with M_*/M_{halo} that is consistent with other baryonic feedback simulations and that there is less scatter in the relation, particularly for the superbubble model as shown in Figure 5.8.

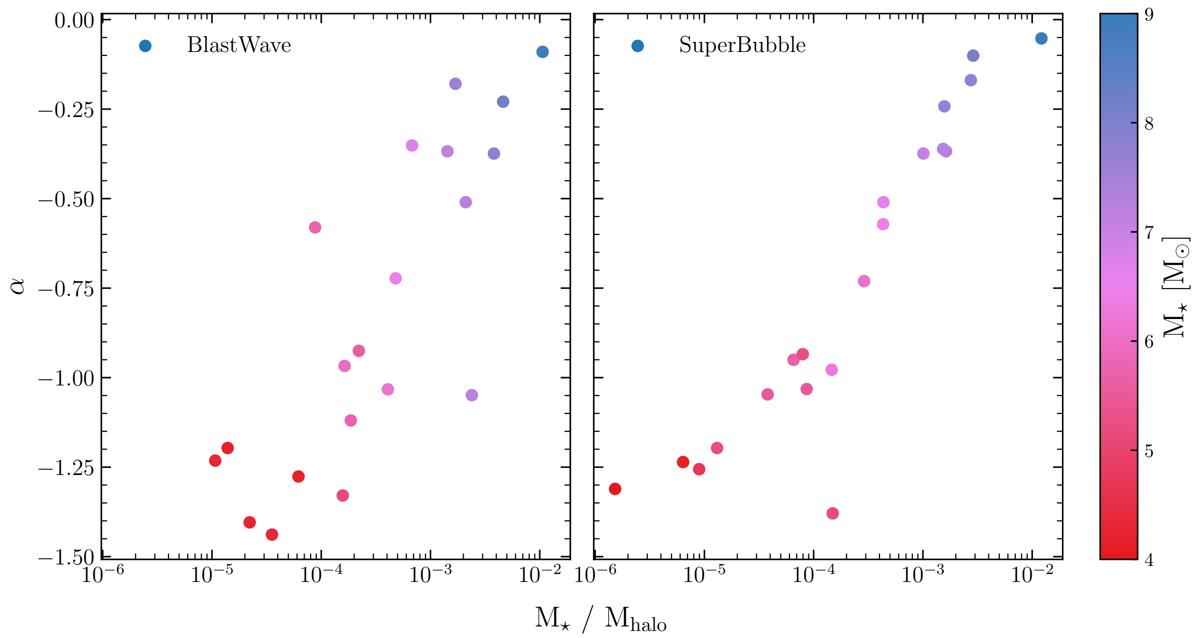

Figure 5.8: α[1-2 %]r_{vir} Core-Einasto core slopes as a function of the stellar mass fraction for the Storm simulations. The superbubble model is less scattered than the blastwave model, indicating a stronger relation to the stellar mass fraction.

5.3. Discussion

As the superbubble model shows more scatter in mean burstiness for the UFD mass range over the entire timescale, it is worth noting that this may be a consequence of feedback implementation. Superbubble feedback run with ChaNGa is shown to reduce stellar mass in Milky-Way size galaxies relative to the blastwave model (Keller et al., 2015). Keller et al. (2014) and Mina et al. (2021) find that the SMHM relation for dwarf galaxies varies with superbubble feedback. A larger sample size may be necessary to determine systematic effects of superbubble feedback following the work of Munshi et al. (2019), that used 100 runs of an individual halo to study the effects of blastwave feedback on dwarf galaxy masses, and considers additional feedback details such as ionizing radiation, ISM turbulence, and runaway massive stars.

As seen in figure 5.4, burstiness generally scales with the stellar mass fraction. For both SN feedback models UFDs form the bulk of their stars in very few major bursts at early times before becoming quenched. Bright dwarfs are seen to be star forming for much longer and are shown to have a more uniform distribution of star formation. Similarly, Emami et al. (2019) find that galaxies below $M_* \sim 10^{7.5}$ $M_\odot$ undergo large, rapid bursts with timescales $\tau < 30$ Myr while galaxies above $M_* \sim 10^{8.5}$ $M_\odot$ have smaller, slower bursts with timescales $\tau \gtrsim 300$ Myr.

It is important to note that the burstiness values in this work are never greater than around -0.4. This is due to the fact that burstiness values are dependent on the binning chosen for the supernova rate. Time is binned in 1 Myr intervals to be consistent with the timing of supernovae feedback in the Storm simulations. The burstiness calculations are averaged over a windowed timescale of 50 Myr to be consistent with the cooling shut-off time period for feedback in our simulations. If the time binning is altered, a windowed timescale over which burstiness is averaged, burstiness values change. This is shown in Figure 5.9, where increasing the timescale to half of the Hubble time increases burstiness values for all halos, with the maximum value going above -0.4. Decreasing the timescale to 1 Myr results in lower burstiness values for all halos.

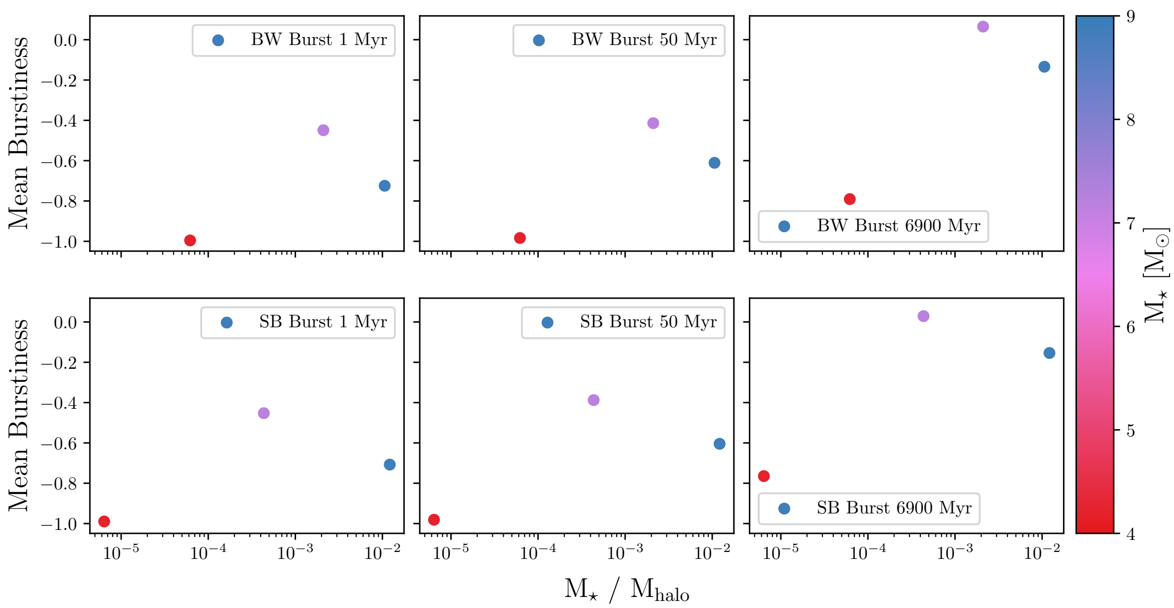

Figure 5.9: Burstiness values averaged over varying timescales. Rows separate feedback models and columns separate the varying timescales over which burstiness is averaged. The middle column shows the 50 Myr timescale used in this work for comparison against other timescales. The data points for all panels are the halos that had the minimum, a middle range value, and the maximum burstiness values for the 50 Myr timescale. Increasing the timescale to half of the Hubble time shows burstiness increasing for all halos, with the maximum value above -0.4. Decreasing the timescale to 1 Myr shows lower burstiness values for all halos.

In addition, far-ultraviolet (FUV) and H_α emissions can be used to quantify the burstiness of observed galaxies. Recently, Flores Velázquez et al. (2021) and Parul et al. (2023) used star formation indicators to measure the burstiness of galaxies from the FIRE project simulations. They found that Milky-Way mass galaxies have highly bursty star formation at early times and time-steady SFR at later times. Future measurements of galaxy SFHs in the local Universe will provide further constraints on the burstiness of dwarf galaxies and can be compared to the results of this work.

Future improvements to the observed stellar mass fraction as a function of halo mass will provide additional constraints on early stellar feedback (Read & Erkal, 2019; Revaz & Jablonka, 2018). Smith (2021) find that adopting IMF averaged rates produces simulations that overestimate the impact of radiation from photo-ionization. However, when compared with explicitly sampling the IMF, an averaged sampling was found to trigger SNe identically in the case where SNe were the only source of feedback. Additionally, Applebaum et al. (2020) show that a stochastic initial mass function (IMF) results in burstier feedback that quenches star formation at earlier times for UFDs.

The Storm simulations were run with the identical UV background, making the comparison of the SN feedback model robust. However, as discussed in Munshi et al. (2019, 2021), many of the low mass halos in the H_2 star formation model are not able to form stars before reionization prevents them from doing so. This implies that the results of this work are sensitive to the selected reionization model. This work adopted the UV background model of Haardt & Madau (2012) that has been shown to heat the IGM earlier ($z \sim 15$) than it should (Oñorbe et al., 2015), potentially making the impact of reionization particularly strong on these results. A more realistic reionization model may allow dark halos in the lower density regions of the Storm simulations to form stars, allowing UFD halos to experience longer quenching times. Benitez-Llambay & Frenk (2020) determined that the effect of reionization on the $z = 0$ occupation fraction varies with how early or late reionization begins. Understanding the impact of reionization will require further simulations and study, but will be essential to determine uncertainties on observational signatures and interpreting VRO's LSST observations.

To expand upon this work, future MARVEL simulations would benefit from investigating the burstiness-core slope relation with respect to M_*/M_{halo}. This would be achieved by examining the effects of the star formation criteria and star formation efficiency on various properties of the MARVEL galaxies to determine any interactions with feedback that may result in a stronger correlation with core slope formation. The implementation of radiative transfer may significantly alter the results of this work, as modeling a realistic ISM would impact the interplay of feedback methodologies and ultimately reshape the DM response. It would also be beneficial to study instantaneous burstiness within the context of reionization, as lower mass halos are unable to form stars due to the non-equilibrium H_2 star formation prescription used in the MARVEL simulations.

Ultimately, this work found that the Storm simulations produce consistent results for higher dwarf galaxy masses regardless of feedback model. The relation between burstiness and DM core slopes remains robust for both models and similar efficiencies for the superbubble model were found within this mass range during active star formation. It also shown that UFDs exhibit similar modeling difficulties that are present in the existing literature and will need to be constrained by future observations by VRO and Roman surveys.

5.4. Conclusion

In summary, the study of bursty star formation in dwarf galaxies reveals critical insights into the interaction between baryonic feedback and DM distributions, showing that feedback can influence the formation of DM cores and address the cusp-core problem that exists within the ΛCDM framework of cosmology. Previous simulations have already implemented baryonic physics, including independent studies and comparisons of blastwave and superbubble feedback for MW-like galaxies and dwarf galaxies. The high resolution of the Storm simulations, however, provides an in-depth comparison of the subgrid physics in these feedback models for a full range of dwarf galaxy masses. This comparison was used to present a novel comparison of the relation between burstiness and DM core slopes using distinct feedback methods. In addition, these results provide new insight on the mass regime of dwarfs that are able to sustain DM cores regardless of feedback model. This chapter underscored the dynamic nature of core formation and core sustainment in low-mass galaxies relative to the burstiness of their star formation, and highlighted the relationship between core slopes and the stellar mass fraction, M_*/M_{halo}. To conclude, Chapter 6 will consolidate the findings from this work and emphasize how the results of this work will guide future research in galaxy simulations and contribute to a broader understanding of modern galaxy evolution within the context of the ΛCDM model and its challenges.

CHAPTER 6

Conclusion

This content of this thesis provided an overview of the cosmological paradigms and emphasizes the significance of the ΛCDM model as the prevailing framework for understanding cosmic evolution. Key challenges such as the missing satellites problem, cusp-core problem, and the too-big-to-fail problem highlight the discrepancies between theoretical predictions and observational data concerning small-scale structures, necessitating physically motivated solutions to resolve these tensions, and in particular, the importance of incorporating baryonic physics into cosmological simulations within the ΛCDM framework.

By understanding the classification and characteristics of dwarf galaxies, their importance as DM-dominated systems is revealed. Categorizing dwarf galaxies by their distinct stellar populations and SFHs emphasizes the role of dwarf galaxies as laboratories for testing CDM models and exploring the interactions between DM and baryonic processes. This work outlined the different methodologies employed in simulating dwarf galaxies, including both N-body and simulations and how hydrodynamics are implemented to model baryons in simulations. In addition, this work highlights the incorporation of baryonic feedback processes in modeling realistic physical interactions that govern star formation and DM dynamics. The importance of simulation resolution in accurately capturing the behavior of dwarf galaxies under different feedback mechanisms.

This work advances the current understanding of dwarf galaxies within the context of the ΛCDM model by comparing the effects of two distinct SN feedback mechanisms, the blastwave and superbubble models, on the cusp-core problem. This work found that regardless of feedback model, a general relation is revealed between bursty star formation and DM cores. In particular, this work presents a novel comparison of core formation and sustainment for a full range of dwarf galaxy masses using distinct feedback methods that implement a star formation prescription that is more physically motivated than other hydrodynamic simulations. This work finds that constraining star formation to the local abundance of molecular hydrogen results in more effective feedback for the higher mass regime of dwarf galaxies, which efficiently form and sustain DM cores throughout the age of the Universe, while the majority of classical and ultra-faint dwarfs retain cuspy DM profiles. Moreover, this work also reveals that UFDs are significantly burstier at high redshift for both feedback models, indicating that this mass regime is sensitive to feedback dynamics and the star formation prescription used in this work.

A comprehensive examination of these feedback models finds that bursty star formation and the resulting baryonic feedback is necessary for dwarf galaxies to sustain their DM cores, and that the stellar mass fraction may better predict DM cores as peak core formation varies with the feedback method. Upcoming surveys from the Rubin Observatory and Roman Space Telescope will be crucial to reach the regime of UFDs, where the majority of theoretical predictions differ. In addition, star formation indicators that can be used to quantify the burstiness of dwarf galaxies in future observations and can provide useful comparisons to this work on the relation between burstiness and DM density profiles.

These insights provide a pathway for further investigation into the nuances of baryonic feedback processes and their implications for DM interactions in low-mass halos. In addition to future surveys, ongoing observations from the Hubble Space Telescope and James Webb Space Telescope will be instrumental in validating the results of this work, improving the implementation of physical processes in cosmological simulations, and providing observational constraints on the properties of dwarf galaxies. This work hopes to strengthen the viability of simulations that operate within the ΛCDM framework by reproducing the observed properties of dwarf galaxies, particularly the distribution of DM and density profiles that would resolve tension with the cusp-core problem. The results of this work contribute to modern galaxy evolution by highlighting the current strengths and weaknesses of dwarf galaxy simulations and how these structures inform our understanding of the nature of DM and its role in shaping the Universe.

Bibliography

Agertz, O., Moore, B., Stadel, J., et al. 2007, MNRAS, 380, 963, doi: 10.1111/j.1365-2966.2007.12183.x

Alpher, R. A., Bethe, H., & Gamow, G. 1948, Phys. Rev., 73, 803, doi: 10.1103/PhysRev.73.803

Applebaum, E., Brooks, A. M., Christensen, C. R., et al. 2021, ApJ, 906, 96, doi: 10.3847/1538-4357/abcafa

Applebaum, E., Brooks, A. M., Quinn, T. R., & Christensen, C. R. 2020, MNRAS, 492, 8, doi: 10.1093/mnras/stz3331

Azartash-Namin, B., Engelhardt, A., Munshi, F., et al. 2024, ApJ, 970, 40, doi: 10.3847/1538-4357/ad49a5

Bakosi, J. 2024, Computer Methods in Applied Mechanics and Engineering, 418, 116586, doi: 10.1016/j.cma.2023.116586

Baumann, D. 2009, arXiv e-prints, arXiv:0907.5424, doi: 10.48550/arXiv.0907.5424

Bekki, K., Couch, W. J., Drinkwater, M. J., & Shioya, Y. 2003, Monthly Notices of the Royal Astronomical Society, 344, 399, doi: 10.1046/j.1365-8711.2003.06916.x

Bellovary, J., Volonteri, M., Governato, F., et al. 2011, ApJ, 742, 13, doi: 10.1088/0004-637X/742/1/13

Bellovary, J. M., Cleary, C. E., Munshi, F., et al. 2019, MNRAS, 482, 2913, doi: 10.1093/mnras/sty2842

Benitez-Llambay, A., & Frenk, C. 2020, MNRAS, 498, 4887, doi: 10.1093/mnras/staa2698

Bennett, C. L., Larson, D., Weiland, J. L., et al. 2013, ApJS, 208, 20, doi: 10.1088/0067-0049/208/2/20

Bertschinger, E. 1995, Cosmological dynamics, Technical Report, Massachusetts Inst. of Tech. Cambridge, MA United States Dept. of Physics., doi: 10.48550/arXiv.astro-ph/9503125

—. 2006, , 74, 063509, doi: 10.1103/PhysRevD.74.063509

Bordner, J., & Norman, M. L. 2018, arXiv e-prints, arXiv:1810.01319, doi: 10.48550/arXiv.1810.01319

Boyanovsky, D. 2021, Universe, 7, doi: 10.3390/universe7080264

Boyarsky, A., Lesgourgues, J., Ruchayskiy, O., & Viel, M. 2009, JCAP, 2009, 012, doi: 10.1088/1475-7516/2009/05/012

Boylan-Kolchin, M., Bullock, J. S., & Kaplinghat, M. 2011, MNRAS, 415, L40, doi: 10.1111/j.1745-3933.2011.01074.x

—. 2012, MNRAS, 422, 1203, doi: 10.1111/j.1365-2966.2012.20695.x

Brook, C. B., & Di Cintio, A. 2015, MNRAS, 450, 3920, doi: 10.1093/mnras/stv864

Brook, C. B., Kawata, D., Gibson, B. K., & Flynn, C. 2004, MNRAS, 349, 52, doi: 10.1111/j.1365-2966.2004.07464.x

Brook, C. B., Governato, F., Roškar, R., et al. 2011, MNRAS, 415, 1051, doi: 10.1111/j.1365-2966.2011.18545.x

Brooks, A. M., Kuhlen, M., Zolotov, A., & Hooper, D. 2013, ApJ, 765, 22, doi: 10.1088/0004-637X/765/1/22

Brooks, A. M., & Zolotov, A. 2014a, ApJ, 786, 87, doi: 10.1088/0004-637X/786/2/87

—. 2014b, ApJ, 786, 87, doi: 10.1088/0004-637X/786/2/87

Brown, T. M., Tumlinson, J., Geha, M., et al. 2014, MmSAI, 85, 493, doi: 10.48550/arXiv.1310.0824

Bryan, G. L., & Norman, M. L. 1998, ApJ, 495, 80, doi: 10.1086/305262

Buchert, T. 2000, in Proceedings of 9th Workshop on General Relativity and Gravitation conference, 306–321, doi: 10.48550/arXiv.gr-qc/0001056

Bullock, J. S., & Boylan-Kolchin, M. 2017, ARA&A, 55, 343, doi: 10.1146/annurev-astro-091916-055313

Bullock, J. S., Kravtsov, A. V., & Weinberg, D. H. 2000, ApJ, 539, 517, doi: 10.1086/309279

Chan, T. K., Kereš, D., Oñorbe, J., et al. 2015, MNRAS, 454, 2981, doi: 10.1093/mnras/stv2165

Christensen, C., Quinn, T., Governato, F., et al. 2012, MNRAS, 425, 3058, doi: 10.1111/j.1365-2966.2012.21628.x

Christensen, C. R., Governato, F., Quinn, T., et al. 2014, MNRAS, 440, 2843, doi: 10.1093/mnras/stu399

Cruz, A., Pontzen, A., Volonteri, M., et al. 2021, MNRAS, 500, 2177, doi: 10.1093/mnras/staa3389

Cushman, P., Galbiati, C., McKinsey, D. N., et al. 2013, arXiv e-prints, arXiv:1310.8327, doi: 10.48550/arXiv.1310.8327

de Blok, W. J. G., McGaugh, S. S., Bosma, A., & Rubin, V. C. 2001, ApJL, 552, L23, doi: 10.1086/320262

de Blok, W. J. G., Walter, F., Brinks, E., et al. 2008, AJ, 136, 2648, doi: 10.1088/0004-6256/136/6/2648

Di Cintio, A., Brook, C. B., Macciò, A. V., et al. 2014, MNRAS, 437, 415, doi: 10.1093/mnras/stt1891

Dodelson, S., & Widrow, L. M. 1994, , 72, 17, doi: 10.1103/PhysRevLett.72.17

Dolag, K., Borgani, S., Schindler, S., Diaferio, A., & Bykov, A. M. 2008, SSRv, 134, 229, doi: 10.1007/s11214-008-9316-5

Dubinski, J., & Carlberg, R. G. 1991, ApJ, 378, 496, doi: 10.1086/170451

Dutton, A. A., Macciò, A. V., Buck, T., et al. 2019, MNRAS, 486, 655, doi: 10.1093/mnras/stz889

Eckert, D., Ettori, S., Robertson, A., et al. 2022, A&A, 666, A41, doi: 10.1051/0004-6361/202243205

Efstathiou, G., Moody, S., Peacock, J. A., et al. 2002, MNRAS, 330, L29, doi: 10.1046/j.1365-8711.2002.05215.x

Einstein, A. 1917, Sitzungsber. Preuss. Akad. Wiss. Berlin (Math. Phys.), 1917, 142

Eisenstein, D. J., & Hu, W. 1998, ApJ, 496, 605, doi: 10.1086/305424

Emami, N., Siana, B., Weisz, D. R., et al. 2019, ApJ, 881, 71, doi: 10.3847/1538-4357/ab211a

Feng, J. L., & Kumar, J. 2008, , 101, 231301, doi: 10.1103/PhysRevLett.101.231301

Flores, R. A., & Primack, J. R. 1994, ApJL, 427, L1, doi: 10.1086/187350

Flores Velázquez, J. A., Gurvich, A. B., Faucher-Giguère, C.-A., et al. 2021, MNRAS, 501, 4812, doi: 10.1093/mnras/staa3893

Frenk, C. S., White, S. D. M., Bode, P., et al. 1999, ApJ, 525, 554, doi: 10.1086/307908

Fry, A. B., Governato, F., Pontzen, A., et al. 2015, MNRAS, 452, 1468, doi: 10.1093/mnras/stv1330

Garrison-Kimmel, S., Boylan-Kolchin, M., Bullock, J. S., & Lee, K. 2014, MNRAS, 438, 2578, doi: 10.1093/mnras/stt2377

Garrison-Kimmel, S., Hopkins, P. F., Wetzel, A., et al. 2019, MNRAS, 487, 1380, doi: 10.1093/mnras/stz1317

Gill, S. P. D., Knebe, A., & Gibson, B. K. 2004, MNRAS, 351, 399, doi: 10.1111/j.1365-2966.2004.07786.x

Gingold, R. A., & Monaghan, J. J. 1977, Monthly Notices of the Royal Astronomical Society, 181, 375, doi: 10.1093/mnras/181.3.375

Governato, F., Brook, C., Mayer, L., et al. 2010a, Nature, 463, 203, doi: 10.1038/nature08640

—. 2010b, Nature, 463, 203, doi: 10.1038/nature08640

Governato, F., Zolotov, A., Pontzen, A., et al. 2012, MNRAS, 422, 1231, doi: 10.1111/j.1365-2966.2012.20696.x

Governato, F., Weisz, D., Pontzen, A., et al. 2015, MNRAS, 448, 792, doi: 10.1093/mnras/stu2720

Guedes, J., Callegari, S., Madau, P., & Mayer, L. 2011, ApJ, 742, 76, doi: 10.1088/0004-637X/742/2/76

Guth, A. H. 1981, Phys. Rev. D, 23, 347, doi: 10.1103/PhysRevD.23.347

Haardt, F., & Madau, P. 2012, ApJ, 746, 125, doi: 10.1088/0004-637X/746/2/125

Hodge, P. W. 1971, ARA&A, 9, 35, doi: 10.1146/annurev.aa.09.090171.000343

Homma, D., Chiba, M., Komiyama, Y., et al. 2024, Publications of the Astronomical Society of Japan, 76, 733, doi: 10.1093/pasj/psae044

Hu, W., & White, M. 2004, Scientific American, 290, 44, doi: 10.1038/scientificamerican0204-44

Jackson, R. A., Kaviraj, S., Yi, S. K., et al. 2024, MNRAS, 528, 1655, doi: 10.1093/mnras/stae056

Jahn, E. D., Sales, L. V., Marinacci, F., et al. 2023, MNRAS, 520, 461, doi: 10.1093/mnras/stad109

Jetley, P., Kale, L. V., Gioachin, F., Quinn, T., & Mendes, C. 2008, in 2008 IEEE International Parallel Distributed Processing Symposium (Los Alamitos, CA, USA: IEEE Computer Society), 1–12, doi: 10.1109/IPDPS.2008.4536319

Kale, L. V., & Krishnan, S. 1993, in Proceedings of the Eighth Annual Conference on Object-Oriented Programming Systems, Languages, and Applications, OOPSLA '93 (New York, NY, USA: Association for Computing Machinery), 91–108, doi: 10.1145/165854.165874

Katz, N. 1992, ApJ, 391, 502, doi: 10.1086/171366

Keller, B. W. 2022, ApJ, 939, 4, doi: 10.3847/1538-4357/ac92fe

Keller, B. W., Wadsley, J., Benincasa, S. M., & Couchman, H. M. P. 2014, MNRAS, 442, 3013, doi: 10.1093/mnras/stu1058

Keller, B. W., Wadsley, J., & Couchman, H. M. P. 2015, MNRAS, 453, 3499, doi: 10.1093/mnras/stv1789

Kennicutt, Robert C., J. 1998, ApJ, 498, 541, doi: 10.1086/305588

Kim, J. E., & Carosi, G. 2010, Reviews of Modern Physics, 82, 557, doi: 10.1103/RevModPhys.82.557

Klypin, A., Kravtsov, A. V., Valenzuela, O., & Prada, F. 1999, ApJ, 522, 82, doi: 10.1086/307643

Knollmann, S. R., & Knebe, A. 2009, ApJS, 182, 608, doi: 10.1088/0067-0049/182/2/608

Koposov, S., Belokurov, V., Evans, N. W., et al. 2008, ApJ, 686, 279, doi: 10.1086/589911

Kroupa, P. 2001, MNRAS, 322, 231, doi: 10.1046/j.1365-8711.2001.04022.x

Landau, L. D., & Lifshitz, E. M. 1959, Fluid mechanics

Laney, C. B. 1998, Computational gasdynamics (Cambridge university press)

Lazar, A., Bullock, J. S., Boylan-Kolchin, M., et al. 2020, MNRAS, 497, 2393, doi: 10.1093/mnras/staa2101

Lemaitre, G. 1934, Proceedings of the National Academy of Science, 20, 12, doi: 10.1073/pnas.20.1.12

Leveque, R. J., Mihalas, D., Dorfi, E. A., & Müller, E. 1999, Irish Astronomical Journal, 26, 73

Linder, E. V. 2017, , 95, 023518, doi: 10.1103/PhysRevD.95.023518

Lucy, L. B. 1977, AJ, 82, 1013, doi: 10.1086/112164

Mateo, M. L. 1998, ARA&A, 36, 435, doi: 10.1146/annurev.astro.36.1.435

McConnachie, A. W., & Irwin, M. J. 2006, MNRAS, 365, 902, doi: 10.1111/j.1365-2966.2005.09771.x

McKee, C. F., & Ostriker, J. P. 1977, ApJ, 218, 148, doi: 10.1086/155667

Menon, H., Wesolowski, L., Zheng, G., et al. 2015, Computational Astrophysics and Cosmology, 2, 1, doi: 10.1186/s40668-015-0007-9

Mina, M., Shen, S., Keller, B. W., et al. 2021, A&A, 655, A22, doi: 10.1051/0004-6361/202039420

Mo, H., Van den Bosch, F., & White, S. 2010, Galaxy formation and evolution (Cambridge University Press)

Monaghan, J. J. 1992, ARA&A, 30, 543, doi: 10.1146/annurev.aa.30.090192.002551

Moore, B. 1994, Nature, 370, 629, doi: 10.1038/370629a0

Moore, B., Ghigna, S., Governato, F., et al. 1999, ApJL, 524, L19, doi: 10.1086/312287

Müller, O., Pawlowski, M. S., Lelli, F., et al. 2021, A&A, 645, L5, doi: 10.1051/0004-6361/202039973

Munshi, F., Brooks, A. M., Applebaum, E., et al. 2021, ApJ, 923, 35, doi: 10.3847/1538-4357/ac0db6

Munshi, F., Brooks, A. M., Christensen, C., et al. 2019, ApJ, 874, 40, doi: 10.3847/1538-4357/ab0085

Munshi, F., Governato, F., Brooks, A. M., et al. 2013, ApJ, 766, 56, doi: 10.1088/0004-637X/766/1/56

Nath, B. B., & Shchekinov, Y. 2013, The Astrophysical Journal, 777, L12, doi: 10.1088/2041-8205/777/1/l12

Navarro, J. F., Eke, V. R., & Frenk, C. S. 1996, MNRAS, 283, L72, doi: 10.1093/mnras/283.3.L72

Navarro, J. F., Frenk, C. S., & White, S. D. M. 1997, ApJ, 490, 493, doi: 10.1086/304888

Navarro, J. F., Hayashi, E., Power, C., et al. 2004, MNRAS, 349, 1039, doi: 10.1111/j.1365-2966.2004.07586.x

Nelson, D., Pillepich, A., Genel, S., et al. 2015, Astronomy and Computing, 13, 12, doi: 10.1016/j.ascom.2015.09.003

Niemeyer, J. C. 2020, Progress in Particle and Nuclear Physics, 113, 103787, doi: 10.1016/j.ppnp.2020.103787

Oñorbe, J., Boylan-Kolchin, M., Bullock, J. S., et al. 2015, MNRAS, 454, 2092, doi: 10.1093/mnras/stv2072

Oman, K. A., Navarro, J. F., Sales, L. V., et al. 2016, MNRAS, 460, 3610, doi: 10.1093/mnras/stw1251

Oman, K. A., Navarro, J. F., Fattahi, A., et al. 2015, MNRAS, 452, 3650, doi: 10.1093/mnras/stv1504

Ostriker, J. P., & Peebles, P. J. E. 1973, ApJ, 186, 467, doi: 10.1086/152513

Parul, H., Bailin, J., Wetzel, A., et al. 2023, MNRAS, 520, 1672, doi: 10.1093/mnras/stad206

Pawlowski, M. S., & Kroupa, P. 2020, MNRAS, 491, 3042, doi: 10.1093/mnras/stz3163

Peebles, P. J. E. 1980a, The large-scale structure of the universe

—. 1980b, The large-scale structure of the universe

Peebles, P. J. E., & Ratra, B. 1988, ApJL, 325, L17, doi: 10.1086/185100

Penzias, A. A., & Wilson, R. W. 1965, ApJ, 142, 419, doi: 10.1086/148307

Perlmutter, S., Aldering, G., Goldhaber, G., et al. 1999, ApJ, 517, 565, doi: 10.1086/307221

Peterson, C. J., Rubin, V. C., Ford, W. K., J., & Roberts, M. S. 1978, ApJ, 226, 770, doi: 10.1086/156658

Phillips, J. C., Hardy, D. J., Maia, J. D. C., et al. 2020, The Journal of Chemical Physics, 153, 044130, doi: 10.1063/5.0014475

Planck Collaboration, Aghanim, N., Akrami, Y., et al. 2020, A&A, 641, A6, doi: 10.1051/0004-6361/201833910

Pontzen, A., & Governato, F. 2012, MNRAS, 421, 3464, doi: 10.1111/j.1365-2966.2012.20571.x

Pontzen, A., Roškar, R., Stinson, G., & Woods, R. 2013, pynbody: N-Body/SPH analysis for python, Astrophysics Source Code Library, record ascl:1305.002

Price, D. J. 2008, Journal of Computational Physics, 227, 10040, doi: 10.1016/j.jcp.2008.08.011

Read, J. I., & Erkal, D. 2019, MNRAS, 487, 5799, doi: 10.1093/mnras/stz1320

Read, J. I., & Gilmore, G. 2005, MNRAS, 356, 107, doi: 10.1111/j.1365-2966.2004.08424.x

Read, J. I., Iorio, G., Agertz, O., & Fraternali, F. 2016, MNRAS, 462, 3628, doi: 10.1093/mnras/stw1876

Relatores, N. C., Newman, A. B., Simon, J. D., et al. 2019, ApJ, 887, 94, doi: 10.3847/1538-4357/ab5305

Revaz, Y., & Jablonka, P. 2018, A&A, 616, A96, doi: 10.1051/0004-6361/201832669

Riess, A. G., Filippenko, A. V., Challis, P., et al. 1998, AJ, 116, 1009, doi: 10.1086/300499

Rocha, M., Peter, A. H. G., Bullock, J. S., et al. 2013, MNRAS, 430, 81, doi: 10.1093/mnras/sts514

Rose, J. C., Torrey, P., Vogelsberger, M., & O'Neil, S. 2022, Monthly Notices of the Royal Astronomical Society, 519, 5623, doi: 10.1093/mnras/stac3634

Rubin, V. C., Ford, W. K., J., & Thonnard, N. 1978, ApJL, 225, L107, doi: 10.1086/182804

Rubin, V. C., & Ford, W. Kent, J. 1970, ApJ, 159, 379, doi: 10.1086/150317

Sales, L. V., Wetzel, A., & Fattahi, A. 2022, Nature Astronomy, 6, 897, doi: 10.1038/s41550-022-01689-w

Sands, I. S., Hopkins, P. F., Shen, X., et al. 2024, arXiv e-prints, arXiv:2404.16247, doi: 10.48550/arXiv.2404.16247

Sawala, T., Frenk, C. S., Crain, R. A., et al. 2013, MNRAS, 431, 1366, doi: 10.1093/mnras/stt259

Sawala, T., Frenk, C. S., Fattahi, A., et al. 2016, MNRAS, 457, 1931, doi: 10.1093/mnras/stw145

Schaye, J., Crain, R. A., Bower, R. G., et al. 2015, MNRAS, 446, 521, doi: 10.1093/mnras/stu2058

Schmidt, B. P. 2012, in American Astronomical Society Meeting Abstracts, Vol. 220, American Astronomical Society Meeting Abstracts #220, 327.01

Schmidt, M. 1959, ApJ, 129, 243, doi: 10.1086/146614

Schneider, A., Anderhalden, D., Maccio, A. V., & Diemand, J. 2014, MNRAS, 441, L6, doi: 10.1093/mnrasl/slu034

Shankaranarayanan, S., & Johnson, J. P. 2022, General Relativity and Gravitation, 54, 44, doi: 10.1007/s10714-022-02927-2

Sharma, P., Roy, A., Nath, B. B., & Shchekinov, Y. 2014, Monthly Notices of the Royal Astronomical Society, 443, 3463, doi: 10.1093/mnras/stu1307

Shen, S., Madau, P., Conroy, C., Governato, F., & Mayer, L. 2014, ApJ, 792, 99, doi: 10.1088/0004-637X/792/2/99

Shen, S., Wadsley, J., & Stinson, G. 2010, MNRAS, 407, 1581, doi: 10.1111/j.1365-2966.2010.17047.x

Silk, J., Di Cintio, A., & Dvorkin, I. 2014, in Proceedings of the International School of Physics 'Enrico Fermi' Course 186 'New Horizons for Observational Cosmology' Vol. 186, Vol. 186, 137–187, doi: 10.3254/978-1-61499-476-3-137

Simon, J. D. 2019, ARA&A, 57, 375, doi: 10.1146/annurev-astro-091918-104453

Simon, J. D., Bolatto, A. D., Leroy, A., Blitz, L., & Gates, E. L. 2005, ApJ, 621, 757, doi: 10.1086/427684

Simon, J. D., & Geha, M. 2007, ApJ, 670, 313, doi: 10.1086/521816

Smith, M. C. 2021, MNRAS, 502, 5417, doi: 10.1093/mnras/stab291

Sohn, S. T., Patel, E., Fardal, M. A., et al. 2020, ApJ, 901, 43, doi: 10.3847/1538-4357/abaf49

Somerville, R. S., & Davé, R. 2015, ARA&A, 53, 51, doi: 10.1146/annurev-astro-082812-140951

Sparre, M., Hayward, C. C., Feldmann, R., et al. 2017, MNRAS, 466, 88, doi: 10.1093/mnras/stw3011

Spergel, D. N., & Steinhardt, P. J. 2000, , 84, 3760, doi: 10.1103/PhysRevLett.84.3760

Spergel, D. N., Bean, R., Doré, O., et al. 2007, ApJS, 170, 377, doi: 10.1086/513700

Springel, V. 2010, ARA&A, 48, 391, doi: 10.1146/annurev-astro-081309-130914

Springel, V., & Hernquist, L. 2002, MNRAS, 333, 649, doi: 10.1046/j.1365-8711.2002.05445.x

—. 2003, MNRAS, 339, 289, doi: 10.1046/j.1365-8711.2003.06206.x

Springel, V., Wang, J., Vogelsberger, M., et al. 2008, MNRAS, 391, 1685, doi: 10.1111/j.1365-2966.2008.14066.x

Springel, V., Pakmor, R., Pillepich, A., et al. 2018, MNRAS, 475, 676, doi: 10.1093/mnras/stx3304

Stinson, G., Seth, A., Katz, N., et al. 2006, MNRAS, 373, 1074, doi: 10.1111/j.1365-2966.2006.11097.x

Tammann, G. A. 1980, in ESA Workshop on Dwarf Galaxies, ed. M. Tarenghi & K. Kjaer, 3

Tasker, E. J., Brunino, R., Mitchell, N. L., et al. 2008, MNRAS, 390, 1267, doi: 10.1111/j.1365-2966.2008.13836.x

Tegmark, M., Strauss, M. A., Blanton, M. R., et al. 2004, , 69, 103501, doi: 10.1103/PhysRevD.69.103501

Teyssier, R. 2002, A&A, 385, 337, doi: 10.1051/0004-6361:20011817

Tollet, E., Macciò, A. V., Dutton, A. A., et al. 2016, MNRAS, 456, 3542, doi: 10.1093/mnras/stv2856

Tolstoy, E., Hill, V., & Tosi, M. 2009, ARA&A, 47, 371, doi: 10.1146/annurev-astro-082708-101650

Tremmel, M., Governato, F., Volonteri, M., & Quinn, T. R. 2015, MNRAS, 451, 1868, doi: 10.1093/mnras/stv1060

Tremmel, M., Karcher, M., Governato, F., et al. 2017a, MNRAS, 470, 1121, doi: 10.1093/mnras/stx1160

—. 2017b, MNRAS, 470, 1121, doi: 10.1093/mnras/stx1160

Viel, M., Becker, G. D., Bolton, J. S., & Haehnelt, M. G. 2013, , 88, 043502, doi: 10.1103/PhysRevD.88.043502

Viel, M., Lesgourgues, J., Haehnelt, M. G., Matarrese, S., & Riotto, A. 2005, , 71, 063534, doi: 10.1103/PhysRevD.71.063534

Wadsley, J. W., Keller, B. W., & Quinn, T. R. 2017, MNRAS, 471, 2357, doi: 10.1093/mnras/stx1643

Wadsley, J. W., Stadel, J., & Quinn, T. 2004, NewA, 9, 137, doi: 10.1016/j.newast.2003.08.004

Weinberg, S. 1989, Rev. Mod. Phys., 61, 1, doi: 10.1103/RevModPhys.61.1

Weisz, D. R., Dolphin, A. E., Skillman, E. D., et al. 2014, ApJ, 789, 147, doi: 10.1088/0004-637X/789/2/147

Wetzel, A. R., Hopkins, P. F., Kim, J.-h., et al. 2016, ApJL, 827, L23, doi: 10.3847/2041-8205/827/2/L23

White, S. D. M., & Rees, M. J. 1978, MNRAS, 183, 341, doi: 10.1093/mnras/183.3.341

Wolf, J., Martinez, G. D., Bullock, J. S., et al. 2010, MNRAS, 406, 1220, doi: 10.1111/j.1365-2966.2010.16753.x

Zolotov, A., Brooks, A. M., Willman, B., et al. 2012, ApJ, 761, 71, doi: 10.1088/0004-637X/761/1/71

CHAPTER A

Appendix 1 Software

This appendix provides descriptions and citations for the software used in this work and the MARVEL simulations.

A.1. CHANGA

CHANGA (Charm N-body GrAvity solver) is a parallel N-Body + SPH code used in cosmological simulations to understand astrophysical processes of galaxy and large-scale structure formation (Jetley et al., 2008). CHANGA uses the CHARM++ infrastructure to use thousands of machine processors and produce simulation scalability that is able to capture astrophysical processes across a wide range of both spatial resolution and varying time scales. The scaling capability of this code is crucial in order for simulations to determine structure formation and model physical processes. As an example, star formation is confined to regions of dense gas that span a few parsecs, whereas the galaxy formation is driven by large-scale structures on the order of megaparsecs (Menon et al., 2015).

CHANGA follows the tree + SPH method of GASOLINE (Wadsley et al., 2004, 2017) to solve the Euler equations of state and implements key cosmological simulation features such as periodic boundary conditions, evolution in comoving coordinates, time-stepping with leapfrog integration, and subgrid recipes for star formation and SNe feedback (Menon et al., 2015). The application of this code was central to producing the metal cooling, H_2 star formation prescription, and feedback methodologies used in this work. Additional information can be found on the official code site:

https://faculty.washington.edu/trq/hpcc/tools/changa.html

The version of CHANGA used in this work can be found at the following GitHub repository that is maintained and distributed by the N-BodyShop:

https://github.com/N-BodyShop/changa

A public version of CHANGA can be found here:

https://github.com/N-BodyShop/changa/releases/tag/v3.5

A.2. CHARM++

CHARM++ is a parallel object-oriented programming framework that is based on C++ and developed by the Parallel Programming Laboratory at the University of Illinois at Urbana-Champaign. The CHARM++ runtime system is used for applications of parallel processing and used in codes that require high-performance and massive scaling across thousands of cores. CHARM++ is widely used for complex fluid dynamics computations, climate modeling, molecular dynamics, and Astrophysics applications due to scalability and ease of use for parallel programming (Bordner & Norman, 2018; Phillips et al., 2020; Bakosi, 2024). More information on the CHARM++ framework can be found here:

https://charmplusplus.org/